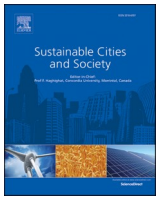
Sustainable Cities and Society 116 (2024) 105880



Contents lists available at ScienceDirect

Sustainable Cities and Society

journal homepage: www.elsevier.com/locate/scs





Assessing diurnal land surface temperature variations across landcover and local climate zones: Implications for urban planning and mitigation strategies on socio-economic factors

Prathiba A. Palanisamy [a,b], Joanna Zawadzka [b,*], Kamal Jain [a], Stefania Bonafoni [c], Anuj Tiwari [d]

[a] Indian Institute of Technology Roorkee, India
[b] Cranfield University, UK
[c] University of Perugia, Italy
[d] Discovery Partners Institute, University of Illinois Systems, Chicago, USA

ARTICLE INFO

Keywords:
Land Surface Temperature
Local Climatic Zones
Land Cover
Socio-economic factors
Diurnal and Multi-temporal Analysis

ABSTRACT

Rising temperatures and rapid urbanization globally reinforce the need to understand urban climates. We investigated the influence of land cover and local climate zones (LCZs) on diurnal land surface temperature (LST) in various seasons in greater Delhi region, India, and their implications on socio-economic factors. Day LST was the highest in the summer and night LST in the monsoon, which also had the lowest diurnal differences in LST. Higher height and density of built-up features contributed to greater heat at night. During the day, open built-up and vegetated areas experienced relatively less heat than their compact equivalents. The lowest diurnal difference was in medium height compact urban zones and tall vegetation. Social inequity in access to urban cooling was indicated by large low-income and heat-vulnerable populations inhabiting the hottest LCZs. This research highlighted that even in semi-arid and subtropical climates, spatial planning policy should consider both the seasonality and diurnal differences in temperature as much as appropriate morphologies for design of thermally comfortable and climate resilient urban spaces. These policies should address the evidenced social inequities in heat exposure to reduce the adverse health impacts on vulnerable groups and therefore contribute to wider societal and economic benefits of healthier populations.

1. Introduction

One of the most evident changes in urban climate caused by rapid population expansion and urbanization is the urban heat island (UHI) phenomenon, where the urban land surface or air temperature is higher than the nearby sub-urban regions (Kumar, Agarwal, Pal, Chandniha & Mishra, 2021; Ullah et al., 2023). The most efficient way to estimate and analyse the fluctuations in surface temperature intensity with respect to seasons, day-night cycles, and local geographical features is to use the land surface temperature (LST) data obtained from remote sensing satellites (Kimothi et al., 2023; Li, Lyu, Chen & Jiang, 2024). Numerous studies have examined the LST as an indication of urbanization-induced climate change at the urban scale (Chauhan & Jethoo, 2023; Y. Chen et al., 2023; Guo et al., 2022; Hamed Fahmy, Amin Abdelfatah & El-Fiky, 2023). These alterations in the urban thermal environment adversely affect the health of city residents of various age groups, encompassing individuals from diverse economic backgrounds (Li, Sun, Li & Gao, 2020; Rydin et al., 2012; Schrijver, Royé, Gasparrini, Franco & Vicedo-Cabrera, 2023).

Urbanization alters the natural land cover (LC) by increasing impervious areas while decreasing forest, agricultural land, and water, resulting in rising LST in urban regions due to increased absorption of solar radiation (Chatterjee & Majumdar, 2022; Morabito et al., 2021; Shahfahad, Naikoo, Towfiqul Islam, Mallick & Rahman, 2022). The difference in temperature between urban and rural areas is particularly apparent on nights with seasons of varying intensity (Dewan, Kiselev & Botje, 2021; Kafy et al., 2022; Siddiqui et al., 2021). Over a 20-year period, changes in land use and land cover (LULC) may raise average metropolitan temperatures by 2 to 10 °C (Abdullah, Barua, Abdullah & Rabby, 2022; Hamed Fahmy et al., 2023; Kafy, Rahman, Faisal, Hasan &

* Corresponding author.
E-mail addresses: pp@ce.iitr.ac.in (P.A. Palanisamy), joanna.zawadzka@cranfield.ac.uk (J. Zawadzka), Kjainfce@iitr.ac.in (K. Jain), stefania.bonafoni@unipg.it (S. Bonafoni), anujt@uic.edu (A. Tiwari).

https://doi.org/10.1016/j.scs.2024.105880
Received 21 April 2024; Received in revised form 3 October 2024; Accepted 5 October 2024
Available online 11 October 2024
2210-6707/© 2024 The Author(s). Published by Elsevier Ltd. This is an open access article under the CC BY license (http://creativecommons.org/licenses/by/4.0/).

Islam, 2020).

In addition to natural landscape change, urbanization significantly changes the morphology and landscape of urban areas, which raises the surface temperature depending on the city scale. Stewart and Oke (2012) developed the local climate zone (LCZ) classification framework to categorize the complex urban area into climate-specific zones based on surface structure, land cover type, and construction materials. The LCZ framework comprises 17 zones with ten built-up classes and seven non-built-up classes with unique features. The urban intensity described by building height and density, land cover, and resulting thermal characteristics manifests in variable LST within the diurnal cycle and seasons, which is primarily apparent in built-up zones (Das & Das, 2020; Du, Chen, Bai & Han, 2020; Unal Cilek & Cilek, 2021). Furthermore, the temperature difference is evident between the zones, with the industrial and built-up-based zones being 4 to 6 °C warmer than the vegetation-based zones during the day (J. Yang et al., 2020). Consequently, evaluating the LST variation within and across different LCZs over different years, seasons and times of day is critical, as this will aid in a more thorough understanding of LST aspects resulting from urban morphology, where past research has trailed.

People migrate from rural to urban areas for economic growth, resulting in high population density in cities. The combined impact of urban heating and increasing surface temperature negatively influence urban populations on various fronts, including economic, social, environmental, and health-related aspects (Chatterjee & Majumdar, 2022; Maharjan et al., 2021). Urban residents are vulnerable to heat stress, which disproportionately affects young people (under 5), the elderly (over 65), and individuals with medical conditions (Das & Das, 2020; Hsu, Sheriff, Chakraborty & Manya, 2021; World Health Organization, 2014). Furthermore, cities are the key contributors to the country's GDP development, accounting for more than 60% of GDP (NITI Aayog & Asian Development Bank, 2022) and recruit a huge floating population. This transient population is generally unaccounted for and faces risks related to heat stress.

The increasing frequency of heat waves and UHI increases mortality rates in cities worldwide (Gao, Hou & Chen, 2019). In Europe, the rapid consequences were observed after extreme occurrences, with a 45% median increase in death risk due to UHI, increasing the monetary burden on the government (Huang et al., 2023). Intergovernmental Panel on Climate Change (2021) reported that under the worst emission scenarios, Delhi, India's National Capital Territory (NCT), temperatures could rise above 35 °C for 187 days a year, or about every other day, and a maximum temperature could increase by 5.3 °C by the end of the century, making it the country's heat capital. In response, governments are taking a variety of short-term remedies, such as providing shelters for the homeless and constructing cold spots during the summer months/heatwave period (Business Standard, 2024). However, long-term planning is more sustainable when incorporating appropriate urban morphology and vegetation into urban planning. analysing socio-demographic data in LCZs aids in resilience planning, targeted mitigation strategies, community engagement and participation, and equitable urban development.

Previous studies have individually examined the seasonal LST and its relationship with LC (Shukla & Jain, 2021; Xian et al., 2022) and LCZs (Kotharkar, Ghosh & Kotharkar, 2021; Parvar, Mohammadzadeh & Saeidi, 2024) or carried out a comparison between cities (Yang et al., 2020; Yuan et al., 2023). Whilst extensively investigating the impact of physical and thermal properties of the land surface on LST, these studies did not directly analyse these in the context of implications for urban planning and mitigation strategies on socio-economic factors. Furthermore, studies have either chosen one year's seasonal data (Du et al., 2020; Yuan, Zhou, Hu & Zhang, 2022; Zheng et al., 2023) to examine LST variations within the land cover/ morphology or performed a temporal analysis to explore the effects of urbanization on LST (Javaid et al., 2023; Zwolska, Półrolniczak & Kolendowicz, 2024). However, the LST of a given season can be influenced by regional weather patterns (Abbasi et al., 2020; Palanisamy, Jain & Bonafoni, 2023; Zhao & Duan, 2020) and policy planning strategies (Feng, Wang, Yuan, Zhang & Yu, 2023; Guha & Govil, 2021) within a given year, which could lead to misunderstandings regarding the association between land features and LST. Furthermore, only a few studies so far have analysed the diurnal thermal effects within LCZs (Wang, Ishida & Mochida, 2023; Xin et al., 2022).

In this study, we address this gap by investigating diurnal variations in LST on an annual and seasonal basis within both different land cover and local climate zones across several years. As such, we do not only determine which land cover types and local climate zones are prone to overheating but also investigate the diurnal differences in LST in the zones in different seasons, which allows for a comprehensive analysis of excess heat formation in different urban morphologies and weather patterns. Furthermore, we relate our findings to the distribution of age-sensitive and economically vulnerable populations within the LCZs to examine their potential exposure to differing diurnal thermal patterns, which has not been explicitly investigated so far for LCZs in the seasonal context. Our focus on an area under a predominantly semi-arid climate with four seasons characterised by distinct humidity and thermal properties allows for drawing conclusions on the possible thermal performance of metropolitan areas with similar land use patterns and climates and where climate shifts are anticipated due to climate change. Therefore, this study provides evidence to urban planners and policy makers for long-term planning of heat-resilient cities as well as tailored heat mitigation strategies that effectively address the challenges faced by different urban morphologies and their associated populations. This study also provides insights as to where emergency services for rapid response to excess heat events could be most needed or where heat respite areas could be created.

Diurnal analysis of LST across different urban morphological features coupled with demographic and socio-economic data is central to international initiatives tackling urbanization challenges, exemplified by the United Nations' advocacy for sustainable cities and communities. Our research directly contributes to the sustainable development goals 11 – Sustainable Cities and Communities, 3 – Good Health and Well-being, and 13 – Climate Action.

2. Materials and methods

2.1. Study area

The study area comprises the National Capital Region (NCR) of India that encompasses the capital city of Delhi and its surrounding satellite towns (Fig. 1), extending between latitudes 28 N and 29.5 N and longitudes 76.5 E and 78 E over 12,700 square kilometers. The main towns included in the study area are Delhi, India's National Capital Territory (NCT) and the neighbouring satellite towns such as Dadri, Gurugram, Faridabad, Ghaziabad, and Meerut. The predominant land cover category in the study region is dense to sparse urban and vegetation cover, hilly terrain, water bodies, and fallow land (Palanisamy, Zawadzka, Jain & Bonafoni, 2023). In the Koppen climate classification system, a significant portion of the study region falls in the hot semi-arid climate region (BSh), and a small portion of the study region in the north-east falls in the monsoon-influenced humid subtropical climate (Cwa). The study region has four major weather patterns, i.e., Winter (December–February), Summer (March–June), Monsoon (July–September), and Post-Monsoon (October–November). Winter has an average temperature and rainfall of 15 °C and 21 mm, summer of 29.5 °C and 32 mm, monsoon of 28.5 °C and 163 mm, and post-monsoon of 23 °C and 9 mm, respectively (Climate data, 2022). Specifically, the winters are cold and dry, where temperatures fall to 2 °C, and the summers are hot and humid, where temperatures rise to 45 °C (Mohan, Sati & Bhati, 2020). Heatwaves are prevalent during summer, particularly in May and June, when temperatures can escalate even further.

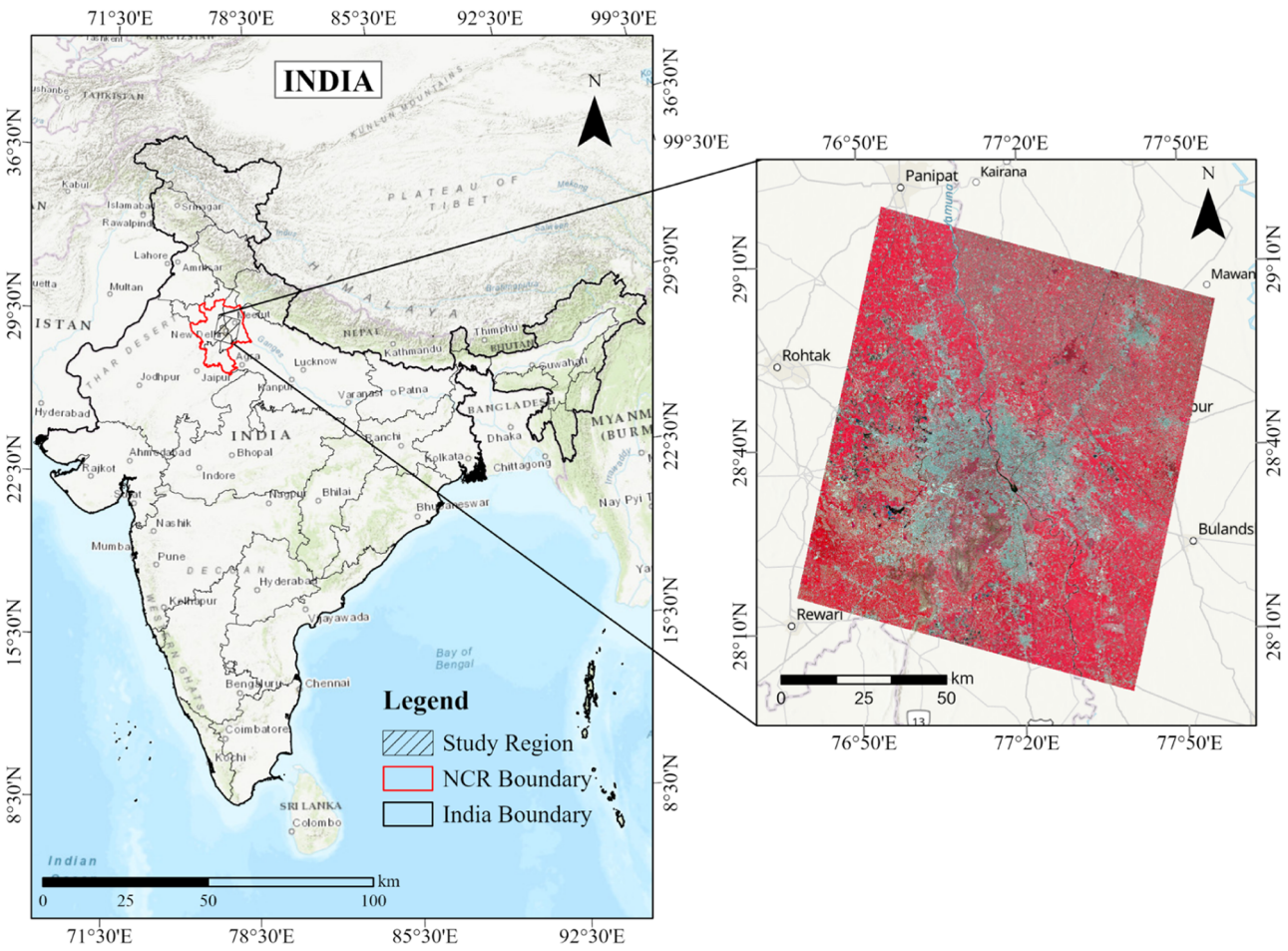


Fig. 1. Location of the study region within India. The false colour composite in the insert represents the spatial distribution of built-up (shades of blue) and vegetated land (shades of red).

2.2. Data

The Google Earth Engine (GEE) platform was used to retrieve satellite imagery representing day and night-time LST (Moderate Resolution Imaging Spectroradiometer - MODIS) as well as inputs for land cover classification (two scenes of Landsat 8 to cover the study area extent). LCZs were obtained from the published global scale urban landscape data at 100 m resolution (Demuzere et al., 2022). GDP [millions of 2017 US dollars] at a spatial resolution of 1 km x 1 km was derived from calibrated night light data for year 2019 by J. Chen et al. (2022). The age structure data adopted here were produced with the Built-Settlement Growth Model (BSGM) (Bondarenko, Kerr, Sorichetta & Tatem, 2020) at 100 m spatial resolution for the year 2020. More information about the data used in the study is given in Table 1. The LCZ, LC, GDP and population data were pre-processed using ArcGIS Pro software. To spatially align age-structured data with LST, fishnets were first constructed at a 1 km spatial resolution of LST, and zonal statistics were used to count the number of individuals in each cell of the fishnet. The GDP data was reprojected and resampled to overlay the pixels over the LST rasters, allowing for direct comparisons.

Table 1
Data used and their description.

S. No	Data	Period	Resolution	Source
1	LST	Daily images – day and night for 2019, 2020, 2021 & 2022	1 km	MOD11A1 V6.1 LST from NASA's Terra and Aqua satellites
2	LC	29.03.2020 04.04.2020	30 m	Landsat 8 by United States Geological Survey
3	LCZ	2020	100 m	(Demuzere et al., 2022)
4	GDP	2019	1 km	(J. Chen et al., 2022)
5	Age Structure	2020	100m	(Bondarenko et al., 2020; WorldPop, 2020)

2.3. Methods

This study was performed in two stages, i.e., data preparation and analysis (Fig. 2). In the data preparation stage, land cover in different LCZs was determined (Section 2.3.1.) and day-time and night-time land surface temperature for different years and seasons was calculated for each LC and LCZ class (Section 2.3.2). In the second stage, statistical analysis of the relationship between the day- and night-time LST and socio-economic factors within LCs and LCZs was carried out.

2.3.1. Land cover classification and LCZs

To examine the relationship between land cover and the LST, the Landsat 8 imagery was used to derive the land cover map with three dominant classes: urban, vegetation and water (Fig. 3a). Although these three classes were required for the study, to increase classification accuracy, the Landsat 8 image was first categorized into seven classes, i.e., dense urban, sparse urban, hilly terrain, water bodies, fallow land, dense vegetation, and sparse vegetation using the RF machine learning

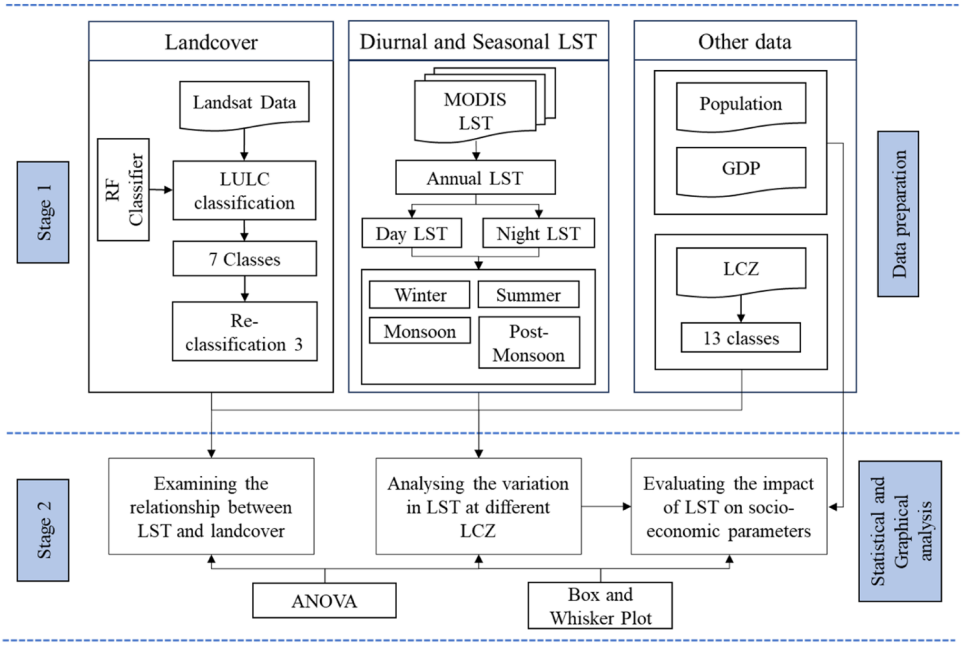


Fig. 2. The methodological framework of the study.

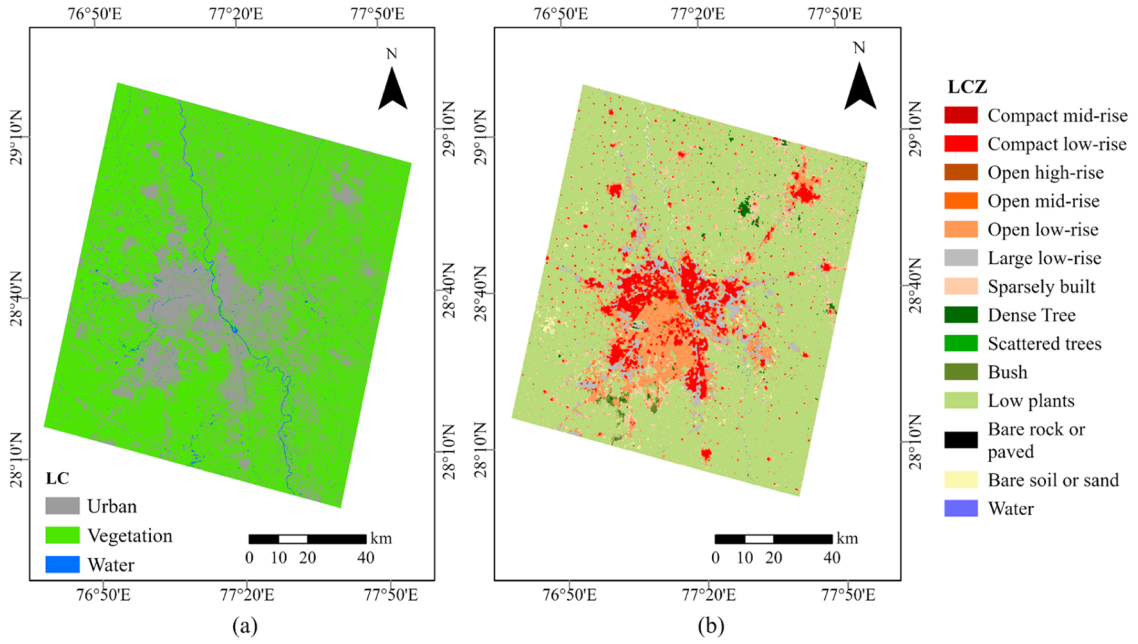


Fig. 3. Land cover classes (a) and local climate zones (b) in the study region.

classifier in the GEE platform Based on our previous study (Palanisamy et al., 2023) the multispectral bands (blue, green, red, NIR, SWIR1 and SWIR2), spectral indices (Normalized Difference Built-up Index (NDBI), Normalized Difference Vegetation Index (NDVI), and Normalized Difference Water Index (NDWI)) and principal components were used as inputs for the classification. The classifiers were trained with 70% of the random samples, while the remaining 30% were used for testing and evaluating performance (Table 2). The accuracy of the resulting map, categorized into seven classes, was assessed by overall accuracy with the result of 79.14%.

The study region comprised 14 LCZs as mapped by Demuzere et al. (2022) at 100 m spatial resolution (Table 3), with an equal proportion of seven building-based and seven vegetation-based zones. Each LCZ was

Table 2
The sample numbers for training and testing the land cover classifier.

Sample Collection (70:30)							
Samples	Urban	Urban-Veg	Dense-Veg	Veg	Water Body	Rock	Fallow land
Training samples	105	25	28	102	53	25	56
Test Samples	45	11	12	44	23	11	24
Total Samples	150	35	40	145	75	35	80

attributed to the spatial distribution of the three main land cover classes. LCZs were utilized to investigate their relationship with LST, socioeconomic characteristics, and the existence of dominating land cover in each zone. The plant-based zones were dominated by low plants, which constituted around 71% or 95.15 km^2 of the study area due to rural/-agricultural land presence. The building-based LCZs were dominant in the centre of the study region, where the NCT Delhi and other rapidly urbanizing satellite towns are located (Figure 3(b)). From the building-based LCZs, the open low-rise and compact low-rise zones were most frequent, covering 10% or 13.62 km^2 and 6% or 8.09 km^2 of the study region, respectively. On the other hand, the open high-rise zone was negligibly small and therefore was not considered in the analysis.

2.3.2. Diurnal LST within LC classes and LCZs

The daily MODIS day and night LST and quality bands were retrieved from repositories and processed in the GEE Platform. Quality bands were used to masque the cloud cover in the LST bands separately for the day and night, and the seasonal and annual averages were calculated for each season and year for the different land cover and local climate zones at a spatial resolution of 1 km. Figure S11 in supplementary materials depicts the availability of the cloudless data for each season. Seasonal averages were calculated for the months of December to February for winter, March to June for summer, July to September for monsoon and October to November for post-monsoon. Additionally, diurnal differences in LST in different LC types and LCZs were calculated – all data are shown in Tables S4 and S8 in Supplementary Materials.

2.3.3. Statistical and graphical analysis

Pairwise Wilcoxon analysis of variance (ANOVA), carried out in R software, was used to determine the presence of statistically significant differences in the land cover types and LCZs located within the study region in terms of their thermal properties expressed as daytime and nighttime LST as well as the socio-economic factors considered in this study. The differences were deemed statistically significant at p-value ≤ 0.05, subdivided into four categories: high significant difference ($p \leq 0.001$), moderate significant difference ($p > 0.001$ and ≤ 0.01), and low significant difference ($p > 0.01$ and $p \leq 0.05$), and no significant difference ($p > 0.05$).

Additionally, box and whisker plots were generated using Python in Google Colab notebook to graphically represent the distribution of LST and socio-economic parameters within the LCZ and LC classes, facilitating the comparison of variations within different LCZ and landcover classes as well as determination of the magnitude of differences between different classes.

Table 3
Local climate zones located within the study area and their description. The area was calculated at its original resolution (100 m).

NO	Zones	Area (km^2)	Percentage (%)	Description
1	Compact mid-rise	9.56	0.08	Areas characterized by compact and medium-rise buildings
2	Compact low-rise	767.72	6.05	Areas characterized by compact and low-rise buildings
3	Open high-rise	0.05	0	Areas with high-rise buildings with more open spaces
4	Open mid-rise	51.36	0.4	Areas with open spaces and medium-rise buildings
5	Open low-rise	1299.83	10.24	Areas with open spaces and low-rise building
6	Large low-rise	578.17	4.56	Areas with large open spaces and low-rise buildings
7	Sparsely built	639.12	5.04	Areas with low population density and sparse building structures
8	Dense Tree	53.77	0.42	Areas with thick tree cover and vegetation
9	Scattered trees	18.47	0.15	Areas with scattered tree cover
10	Bush	36.24	0.29	Areas characterized by dense bush or shrub vegetation
11	Low plants	9096.38	71.67	Areas dominated by low-lying vegetation
12	Bare rock or paved	1.63	0.01	Areas with exposed rock surfaces or extensive paving
13	Bare soil or sand	117.71	0.93	Areas with bare ground or sandy surfaces
14	Water	22.31	0.18	Areas comprising water bodies, such as lakes, rivers, or ponds

3. Results

3.1. Land cover distribution within LCZs

Land cover distribution within the LCZs was determined to gain an understanding of the proportion of the three overall land cover classes (urban, vegetation and water) to aid the interpretation of thermal response and socio-economic characteristics of the LCZs (Fig. 4). Out of the built-up LCZs, four were dominated by the urban LC class – compact mid-rise, compact low-rise, open mid-rise and large low-rise, however, only compact mid-rise did not contain much vegetation at all. On the other hand, open low-rise had a nearly equal proportion of vegetated and urban land, and sparsely built areas were dominated by vegetation. Whilst the vegetation-based zones were typically dominated by the vegetated LC class, some urban areas were present, especially in bare rock or paved and bare soil or sand. This could be attributed to the fact that the spectral response in satellite imagery used for LC classification of bare ground, rock and sand is similar to built-up classes, causing urban to be mapped within these semi-natural LCZs. Vegetation and urban were also present in the water class, which could be attributed to several factors. Firstly, LCZs and our LC map were generated at different spatial resolutions (100 m and 30 m, respectively), which, even after coarsening of these datasets to 1 km resolution to match with LST and GDP data, could have caused the incorporation of non-water LC classes in the water LCZ. Moreover, the distribution of water in the study area varies throughout the year due to the presence of rice paddies seasonally inundated by water, and these differences could have been picked up by the land cover dataset on which the LCZs were based.

3.2. Diurnal annual and seasonal LST distribution within different land cover types

In the initial stage of the study, the research focused on analysing the diurnal variation in LST across the different seasons and years, considering the predominant LC classes (urban, vegetation, water) in the study area. Annually, all LC classes exhibited a downward trend towards the year 2021, followed by an increase in the year 2022 in their LST, both at night and during the day (Fig. 5A, Table S1 and S2 in supplementary materials). However, the temperature increase in 2022 was more evident at night; on average, daytime temperatures in 2022 were 1.23 °C cooler than in 2019, while nighttime temperatures were 0.7 °C warmer than in 2019. Urban class was the warmest; however, it had a wide range of LST values, especially at night, suggesting a variability of thermal response in this class. LST of the vegetation LC was lower by 0.61 °C on average than urban during the day (p-value <0.001, Table S2 in supplementary materials) and by 1.09 °C at night (p-value <0.001), with the average diurnal difference of 16.60 °C in urban and 17.09 in vegetated LC. LST of water was similar to that of the vegetated LC during the day (no statistically significant difference) and to urban at night (p-value >0.01 and p-value $\leq$ 0.05) – which we attribute to the presence of mixed pixels in this class.

In terms of seasonal differences, the day-time LST was the highest in the summer, whereas night-time LST was the highest in the monsoon for

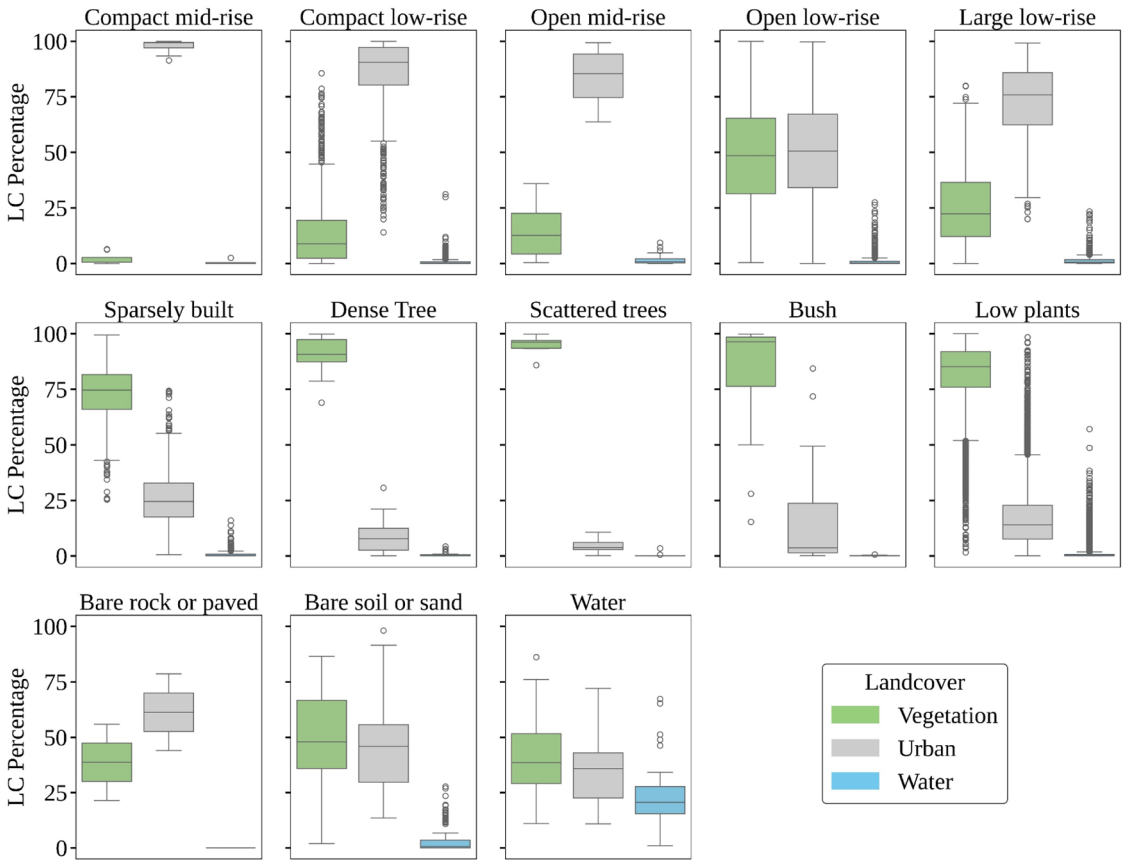


Fig. 4. The distribution of land cover classes within LCZs present in the study area.

all land cover types (Fig. 5B, Table S3 in supplementary materials). The highest recorded daytime temperature was approximately 46 °C during the summer and 28 °C during the monsoon night. On average, however, the daytime summer LST was higher than the monsoon LST by 3.97 °C, 6.6 °C than the post-monsoon and 14.89 °C than winter. Conversely, the nighttime LST in monsoon was higher by 4.34 °C than in the summer, 8.38 °C than in post-monsoon, and 16.01 °C in winter. The differences in the means of LST across the different LC types in the different seasons both during the day and night were statistically significant at p value <0.001, except for the day-time temperatures in vegetation and water, especially in summer and monsoon seasons, with winter and post-monsoon exhibiting a low statistically significant difference (Table 4).

The average diurnal difference in day and night LST across all LC classes was the highest in summer (18.16 °C), followed by post-monsoon (15.61 °C), winter (14.95 °C), and monsoon (9.85 °C) seasons (Table S4 in supplementary materials). When analysed seasonally, the vegetation class exhibited the highest diurnal differences, followed by urban and water, except during the monsoon season. In the monsoon season, the urban class had the highest diurnal difference in LST at 10.31 °C, followed by vegetation at 9.78 °C, and water at 9.47 °C.

The diurnal LST difference was the highest in the summer season, followed by post-monsoon, winter, and monsoon seasons, primarily due to the varying cloud cover percentages. Summer had the least cloud cover, ranging from 10% to 20%, post-monsoon had 10% to 25%, winter ranged from 15% to 23%, and monsoon exceeded 50% (Cloud Cover Data of Delhi, 2018; Sharma, Dass, Mishra, Singh & Kumar, 2022). The cloud cover acts as a blanket and reflects heat back to the surface, resulting in different cooling rates across these seasons (Hu et al., 2021). When studying the cooling rates across different land cover types, vegetation exhibits a higher cooling rate than other classes due to high evapotranspiration (Breil, Davin & Rechid, 2021) and albedo, followed by urban areas and water bodies. However, during the monsoon season, vegetated have a lower cooling rate than urban areas because the high moisture content in the soil and atmosphere due to high humidity reduces evapotranspiration (Denager, Looms, Sonnenborg & Jensen, 2020). Additionally, water bodies retain heat for longer periods due to their high heat storage capacity, exhibiting a slower cooling rate than other classes.

3.3. Annual variation of the day- and night-time LST within local climate zones

Annual patterns of day-time and night-time LST within LCZs exhibited a similar LST trend as the one observed in the LC type analysis (Fig. 4), with temperatures decreasing gradually from 2019 till 2021 and rising in 2022. The decreasing LST trend was more noticeable during the day than at night, with the highest day-time LST observed in 2019 across all LCZs with a mean of 34.45 °C (Table S5 in supplementary materials), 1.56 °C higher than the 2021 LST. In contrast, however, the highest night-time LST was observed in 2022 with 18.03 °C, 0.92 °C higher than the 2021 LST.

Within the built-up based LCZs during the day averaged across 2019–2022, large low-rise (34.62 °C), compact low-rise (34.60 °C), and compact mid-rise (34.33 °C) where the hottest zones, with compact mid-rise not being statistically different from these as well as seemingly cooler zones: open low-rise (33.69 °C) and open mid-rise (33.61 °C), which were not statistically different from each other. Compact low-rise, however, was statistically different from open mid- and low-rise, and large low-rise form open low-rise (Fig. 6, Table S5 and S6 supplementary materials). It needs to be noted that some of the non-urban LCZs had daytime LSTs comparable to the urban zones: bare rock or paved (34.80 °C), bare soil or sand (34.11 °C), and bush (34.08 °C), with no statistically significant differences with the hottest urban zones. The sparsely built LCZ (33.29 °C) was the coolest from the urban LCZs, with some

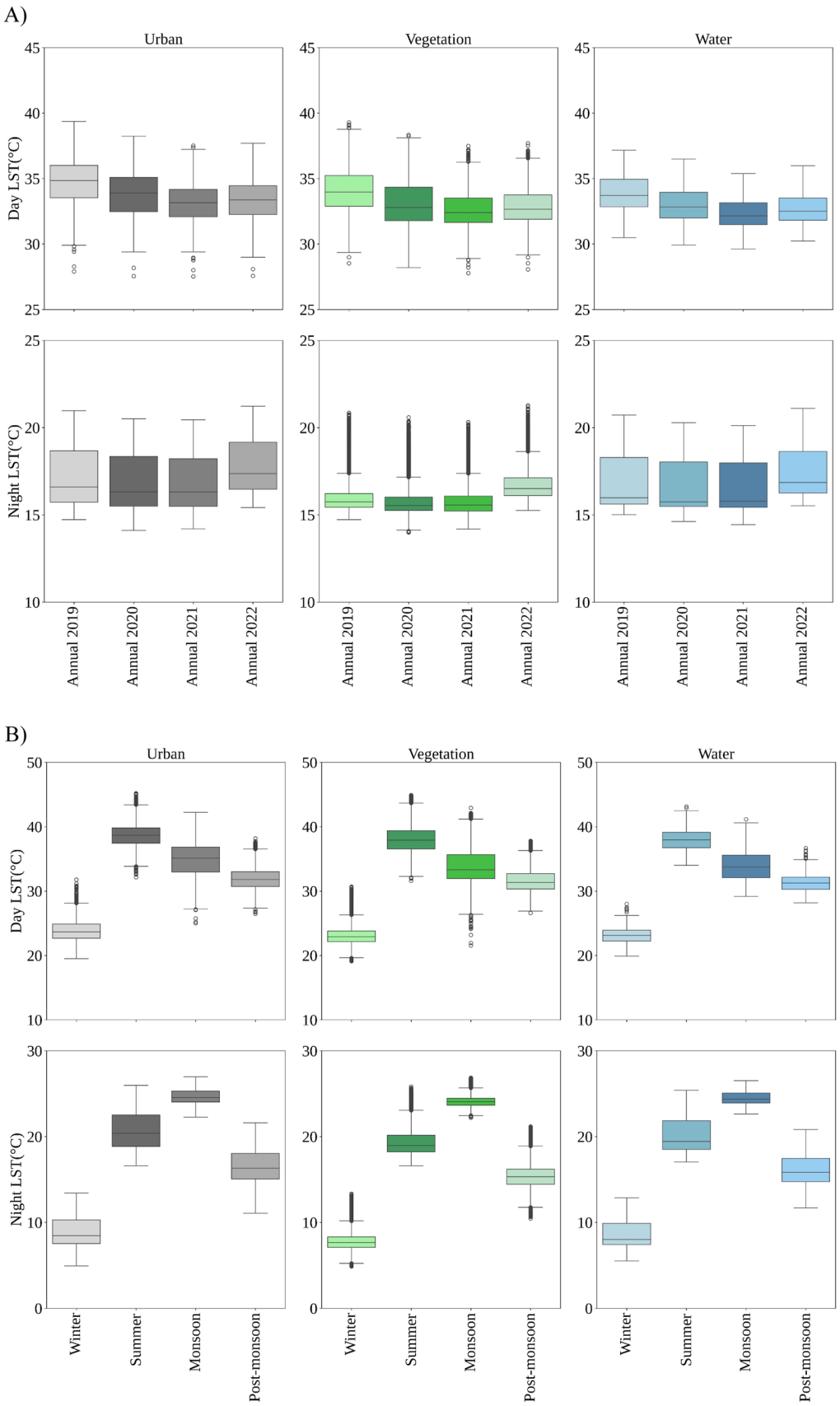


Fig. 5. The annual (A) and seasonal (B) diurnal LST variation in years 2019 – 2022 within the three land cover types considered in this study.

Table 4
The ANOVA analysis of LST within LULC classes. ns - No statistically significant difference, * p-value >0.01 and p-value ≤ 0.05, ** p-value >0.001 and p-value ≤0.01, *** p-value < 0.001.

Season	LC	Day			Night		
		Urban	Vegetation	Water	Urban	Vegetation	Water
Winter	**Urban**	–	–	–	–	–	–
	Vegetation	***	–	–	***	–	–
	Water	***	*	–	***	***	–
Summer	**Urban**	–	–	–	–	–	–
	Vegetation	***	–	–	***	–	–
	Water	***	ns	–	***	***	–
Monsoon	**Urban**	–	–	–	–	–	–
	Vegetation	***	–	–	***	–	–
	Water	***	ns	–	***	***	–
Post-monsoon	**Urban**	–	–	–	–	–	–
	Vegetation	***	–	–	***	–	–
	Water	***	*	–	***	***	–

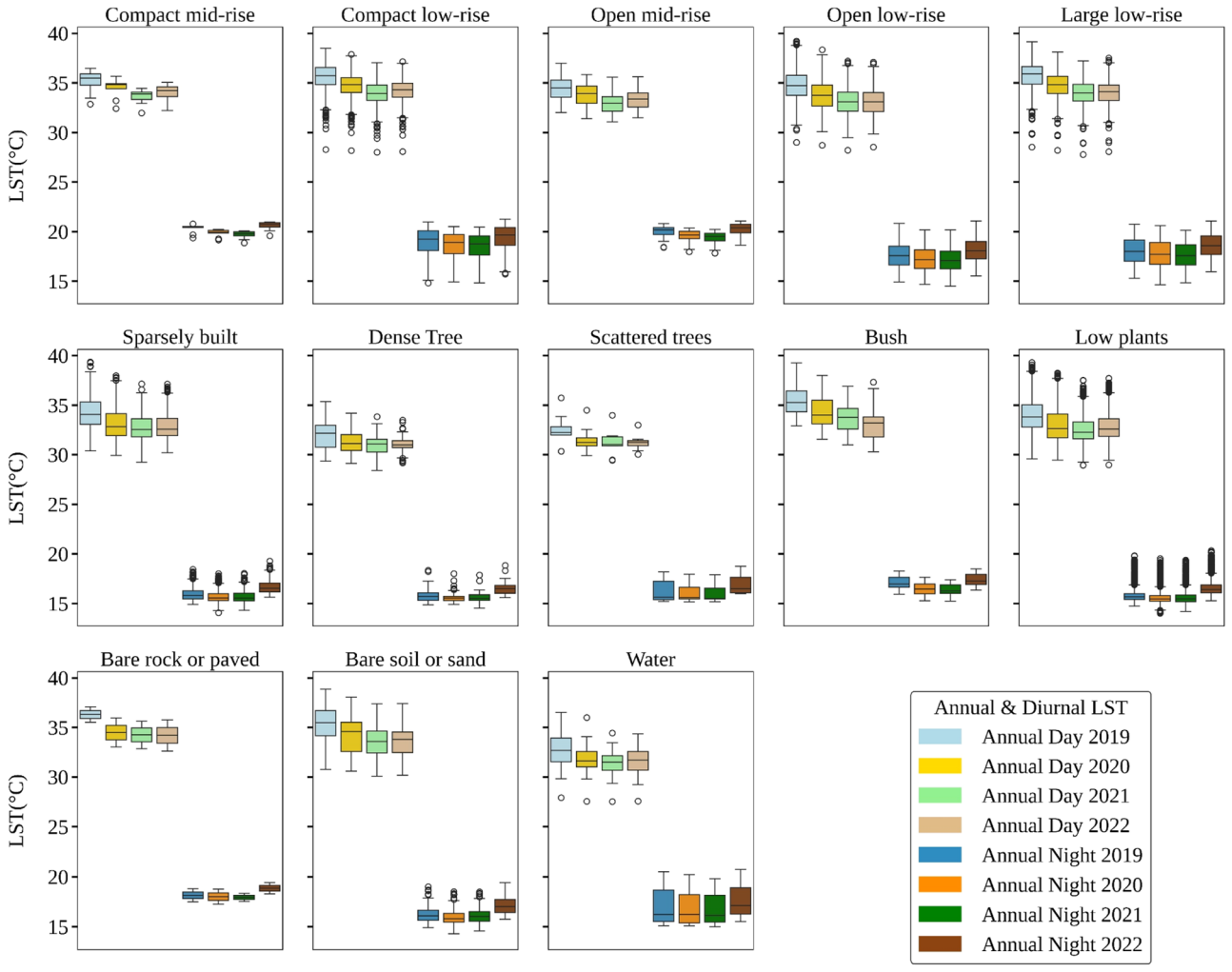


Fig. 6. The annual LST trend from 2019 to 2022 for both day (light colours) and night (dark colours).

similarities with compact mid-rise and open mid-rise, but not in all years. From the non-built-up LCZs, low plants, representing the rural background of the study area, had the highest LST (33.29 °C), which was only statistically different from compact mid-rise at $p < 0.01$ at the most. Water, scattered trees and dense trees with the four-yearly averages ranging between 31.30 - 31.85 °C, were comparable to each other and statistically different from all remaining zones except for bare rock or paved and bare soil or sand in some years.

The differences between the built-up LCZs were more pronounced at night. In the decreasing order from hottest to coolest these were: compact mid-rise (20.10 °C), open mid-rise (19.82 °C, not statistically different to the prior), compact low-rise (18.82 °C), large low-rise (18.02 °C), open low-rise (17.54 °C), and sparsely built (16.01 °C). Bare rock or paved (18.23 °C), which was the hottest during the day, was placed between compact low-rise and open low-rise, and not statistically different form the two. The coolest non-urban LCZ was low plants (15.86 °C), dense trees (15.92 °C), scattered trees (16.30 °C), with no significant differences in the top three, bare soil and sand (16.40 °C), bush

(16.80 °C) and water (16.95 °C). Water was significantly warmer than dense trees and low plants, and significantly cooler than the built-up LCZs. These results imply that LCZs with more open space and lower height of buildings tend to cool down during the night whilst being relatively hot during the day.

In the yearly average, the highest diurnal differences (Table S8 in supplementary materials) were observed in non-built-up zones such as bare soil or sand (15.42 °C), low plants (15.13 °C), water (15.06 °C), and bare rock or paved (14.68 °C). Zones with lower heights of buildings and vegetated features exhibited moderate diurnal differences, including large low-rise (14.63 °C), open low-rise (14.53 °C), bush (14.41 °C), sparsely built (14.2 °C), and compact low-rise (14 °C). Zones with medium height of buildings and taller vegetation had the lowest diurnal differences, such as dense trees (13.6 °C), scattered trees (13.5 °C), open mid-rise (13.2 °C), and compact mid-rise (12.6 °C), however, taller vegetation experienced less heat overall.

3.4. Seasonal variation of the day- and night-time LST within local climate zones

When the seasonal differences in LST, averaged over the 2019–2022 period for the entire study area are concerned, day-time LST was the highest in summer (38.33 °C), followed by monsoon (34.79 °C) post-monsoon (31.58 °C) and winter (23.92 °C) (Table S7A in supplementary materials). At night, however, LST was the highest during the monsoon (24.68 °C), followed by summer (21.04 °C), post-monsoon (16.80 °C) and winter (9.14 °C) (Table S7B in supplementary materials). This pattern transpired throughout all local climate zones (Fig. 7) – winter and post-monsoon LST was the lowest in all LCZs, both during the day and at night whilst summer or monsoon temperatures were the highest depending on time of day. The diurnal difference, across all LCZs, was the highest in the summer (17.29 °C), followed by winter (14.78 °C), post-monsoon (14.77 °C) and monsoon (10.11 °C).

The built-up-based LCZs differed significantly from the non-built-up zones, except for bare rock or paved in all seasons during the night (Table 5), although the pattern was followed only for dense and scattered trees during the day. However, sparsely built showed a very high significant difference between dense trees at day and less between dense trees and scattered trees at night.

On average, during the night, the open mid-rise was 2.5 °C warmer in the summer and 1.1 °C warmer in the monsoon than the open low-rise, and the compact low-rise was 1.33 °C warmer in the summer and 0.73 °C warmer in the monsoon than the open low-rise. During the day, very little difference was seen between mid-rise and low-rise zones, while very little difference was shown between compact and open mid-rise at night. Compact low-rise zones were 1.25 °C warmer than open low-rise zones, and compact mid-rise zones were 1 °C warmer than open mid-rise zones during the day.

No significant difference was observed between the compact low and mid-rise zones during the day in all seasons. However, a very high significant difference was observed at night in the winter, summer, and post-monsoon seasons, as well as a significant difference in the monsoon

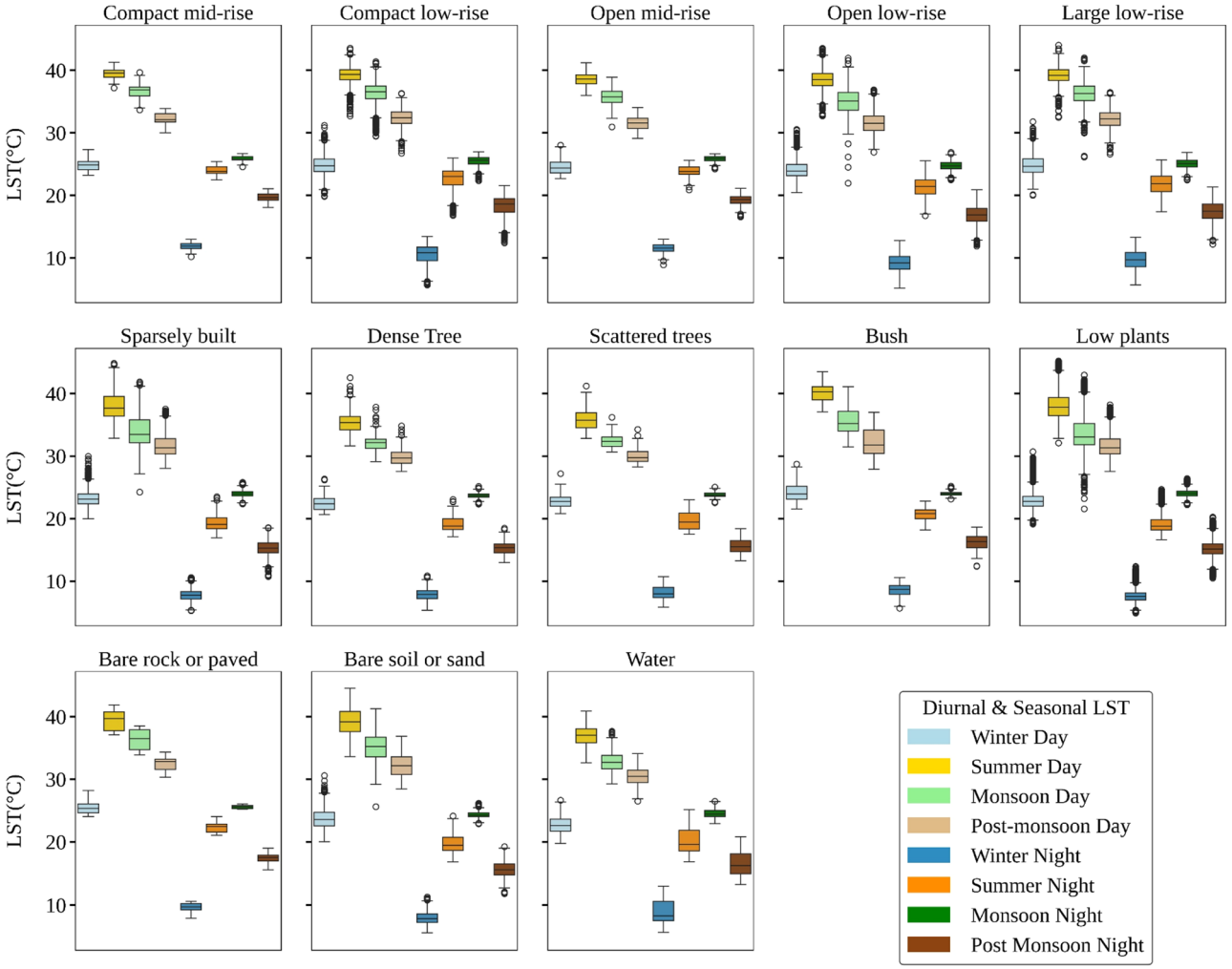


Fig. 7. The variation in day and night LST averaged over seasons from 2019 to 2022 in each LCZ.

Table 5
A day- (A) and night- time (B) ANOVA analysis of LST at different LCZs; W – Winter, S – summer, M – Monsoon and PM – Post-Monsoon, ns – No statistically significant difference, * p-value <0.05, ** p-value < 0.01, *** p-value < 0.001.

Day (A)	Compact mid-rise				Compact low-rise				Open mid-rise				Open low-rise				Large low-rise				Sparsely built				Dense Tree				Scattered trees				Bush				Low plants				Bare rock or paved				Bare soil or sand			
	W	S	M	PM	W	S	M	PM	W	S	M	PM	W	S	M	PM	W	S	M	PM	W	S	M	PM	W	S	M	PM	W	S	M	PM	W	S	M	PM	W	S	M	PM	W	S	M	PM	W	S	M	PM
Compact low-rise	ns	ns	ns	ns	-	-	-	-	-	-	-	-	-	-	-	-	-	-	-	-	-	-	-	-	-	-	-	-	-	-	-	-	-	-	-	-	-	-	-	-	-	-	-	-	-	-
Open mid-rise	*	***	***	**	***	***	***	***	-	-	-	-	-	-	-	-	-	-	-	-	-	-	-	-	-	-	-	-	-	-	-	-	-	-	-	-	-	-	-	-	-	-	-	-	-	-
Open low-rise	***	***	***	**	***	***	***	***	***	ns	***	ns	-	-	-	-	-	-	-	-	-	-	-	-	-	-	-	-	-	-	-	-	-	-	-	-	-	-	-	-	-	-	-	-	-	-
Large low-rise	ns	ns	ns	ns	ns	*	***	***	**	***	***	***	***	***	***	***	-	-	-	-	-	-	-	-	-	-	-	-	-	-	-	-	-	-	-	-	-	-	-	-	-	-	-	-	-	-
Sparsely built	***	***	***	**	***	***	***	***	***	***	***	ns	***	***	***	ns	***	***	***	***	-	-	-	-	-	-	-	-	-	-	-	-	-	-	-	-	-	-	-	-	-	-	-	-	-	-
Dense Tree	***	***	***	***	***	***	***	***	***	***	***	***	***	***	***	***	***	***	***	***	***	***	***	***	-	-	-	-	-	-	-	-	-	-	-	-	-	-	-	-	-	-	-	-	-	-
Scattered trees	***	***	***	***	***	***	***	***	***	***	***	***	***	***	***	***	***	***	***	***	ns	***	***	***	ns	ns	ns	ns	-	-	-	-	-	-	-	-	-	-	-	-	-	-	-	-	-	-
Bush	**	**	**	ns	***	***	***	ns	ns	***	ns	ns	ns	***	ns	*	***	***	***	ns	***	***	***	ns	***	***	***	***	***	***	***	***	-	-	-	-	-	-	-	-	-	-	-	-	-	-
Low plants	***	***	***	**	***	***	***	***	***	***	***	ns	***	***	***	ns	***	***	***	***	***	ns	***	ns	***	***	***	***	ns	***	*	***	***	***	***	*	-	-	-	-	-	-	-	-	-	-	-
Bare rock or paved	ns	ns	ns	ns	ns	ns	ns	ns	*	ns	ns	ns	**	ns	ns	ns	ns	ns	ns	ns	***	ns	**	ns	***	***	***	***	***	**	***	***	*	ns	ns	ns	***	ns	**	ns	-	-	-	-	-	-
Bare soil or sand	***	ns	***	ns	***	ns	***	**	***	***	**	***	***	***	ns	***	***	ns	***	ns	***	***	***	***	***	***	***	***	**	***	***	***	**	***	ns	ns	***	***	***	***	**	ns	ns	ns	-	-	-	-
Water	***	***	***	***	***	***	***	***	***	***	***	***	***	***	***	***	***	***	***	***	***	***	***	***	ns	***	***	***	ns	**	ns	ns	***	***	***	***	ns	***	**	***	***	**	***	**	***	***	***	***

Night (B)	Compact mid-rise				Compact low-rise				Open mid-rise				Open low-rise				Large low-rise				Sparsely built				Dense Tree				Scattered trees				Bush				Low plants				Bare rock or paved				Bare soil or sand			
	W	S	M	PM	W	S	M	PM	W	S	M	PM	W	S	M	PM	W	S	M	PM	W	S	M	PM	W	S	M	PM	W	S	M	PM	W	S	M	PM	W	S	M	PM	W	S	M	PM	W	S	M	PM
Compact low-rise	***	***	**	***	-	-	-	-	-	-	-	-	-	-	-	-	-	-	-	-	-	-	-	-	-	-	-	-	-	-	-	-	-	-	-	-	-	-	-	-	-	-	-	-	-	-
Open mid-rise	*	ns	ns	**	***	***	***	***	-	-	-	-	-	-	-	-	-	-	-	-	-	-	-	-	-	-	-	-	-	-	-	-	-	-	-	-	-	-	-	-	-	-	-	-	-	-
Open low-rise	***	***	***	***	***	***	***	***	***	***	***	***	-	-	-	-	-	-	-	-	-	-	-	-	-	-	-	-	-	-	-	-	-	-	-	-	-	-	-	-	-	-	-	-	-	-
Large low-rise	***	***	***	***	***	***	***	***	***	***	***	***	***	***	***	***	-	-	-	-	-	-	-	-	-	-	-	-	-	-	-	-	-	-	-	-	-	-	-	-	-	-	-	-	-	-
Sparsely built	***	***	***	***	***	***	***	***	***	***	***	***	***	***	***	***	***	***	***	***	-	-	-	-	-	-	-	-	-	-	-	-	-	-	-	-	-	-	-	-	-	-	-	-	-	-
Dense Tree	***	***	***	***	***	***	***	***	***	***	***	***	***	***	***	***	***	***	***	***	ns	*	***	ns	-	-	-	-	-	-	-	-	-	-	-	-	-	-	-	-	-	-	-	-	-	-
Scattered trees	***	***	***	***	***	***	***	***	***	***	***	***	***	***	***	***	***	***	***	***	ns	ns	ns	ns	ns	ns	ns	ns	-	-	-	-	-	-	-	-	-	-	-	-	-	-	-	-	-	-
Bush	***	***	***	***	***	***	***	***	***	***	***	***	***	***	***	***	***	***	***	***	***	***	ns	***	***	***	***	***	ns	***	*	*	-	-	-	-	-	-	-	-	-	-	-	-	-	-
Low plants	***	***	***	***	***	***	***	***	***	***	***	***	***	***	***	***	***	***	***	***	***	***	**	***	***	ns	***	ns	**	*	*	*	***	***	ns	***	-	-	-	-	-	-	-	-	-	-	-
Bare rock or paved	***	***	ns	***	*	ns	ns	ns	***	***	ns	***	ns	ns	***	ns	ns	ns	*	ns	***	***	***	***	***	***	***	***	**	***	***	**	*	***	***	**	***	***	***	***	-	-	-	-	-	-	-
Bare soil or sand	***	***	***	***	***	***	***	***	***	***	***	***	***	***	***	***	***	***	***	***	**	***	***	***	ns	***	***	**	ns	ns	***	ns	***	***	***	***	***	***	***	***	***	***	***	***	-	-	-	-
Water	***	***	***	***	***	***	***	***	***	***	***	***	**	***	***	**	***	***	***	***	***	***	***	***	***	***	***	***	ns	ns	***	*	ns	**	***	ns	***	***	***	***	ns	**	***	ns	***	ns	*	***

season. Overall, the built-up LCZs' LST difference was more noticeable at night than during the day. Buildings classified according to height had a higher night-time LST than the ones classified by density when assessed based on urban morphology. Therefore, these aspects need to be carefully considered during urban planning.

Large low-rise, compact low-rise, compact mid-rise, bush and rock or paved surface zones had the highest LST during the day. Compared to vegetation-based zones and water, compact low-rise, open mid-rise, open low-rise, large low-rise, and sparsely built exhibit significant differences in LST day and night, emphasizing the significance of planting trees in cities to control and lessen LST and alleviate heat stress.

Interestingly, the analysis reveals that compact low-rise zones had higher LST than compact mid-rise zones during the daytime and vice versa at night. The compact zones had higher LST than the open area at night, and a very high significant difference was observed throughout the seasons during the day, highlighting the function of urban morphology in reducing surface temperature. On the other hand, the low-rise zones generally had lower LST than mid-rise zones during the night-time and had a significant temperature difference. The comparison of different zones in urban regions with varying built-up conditions implies that the impact of building density is more important than height in decreasing LST during the day across the seasons.

The natural and low-height feature zones exhibited the highest diurnal temperature differences in the summer compared to all other seasons (Table S8 in supplementary materials). The maximum difference was 19.04 °C in the low plant zone, followed by bare soil or sand at 18.79 °C, and water at 18.38 °C. In contrast, during the monsoon, the higher vegetated feature zones showed less diurnal difference, with dense trees at 8.43 °C and scattered trees at 8.77 °C. The maximum diurnal difference during the monsoon (11.4 °C) was less than the minimum differences observed in other seasons: winter (12.39 °C), summer (15.57 °C), and post-monsoon (12.39 °C).

3.5. Heat exposure of vulnerable populations in local climate zones

Das and Das (2020), Hsu et al. (2021), and World Health Organization (2014) suggested that populations below the age of 5 and above 65 are likely vulnerable to heat. However, for the current study, considering increasing health issues, a buffer of 5 years was applied to both categories. Therefore, vulnerable populations in our study are considered to be children 10 years old or younger, elderly people 60 years old or older, and persons with relatively low income expressed in GDP per capita. These residents are more vulnerable to heat and heat-related diseases due to poor housing and inadequate facilities to prevent heat. The combination of low income and poor thermal environments negatively impacts health, making children, the elderly, and people with existing medical problems particularly vulnerable to heat and heat-related diseases.

Amongst the various LCZs, the built-up zones typically had larger population than those comprising mostly vegetated land (Table S9 in supplementary materials). The highest total population was observed in compact low-rise (13.4 mln), followed by open low-rise (9.6 mln), and large low-rise (5.8 mln). However, the low plants LCZ, which is a predominantly rural zone, comprised the third largest population (8.4 mln), which was likely due to its size, comprising 71.41% of the study region.

The highest proportion of children and the elderly, as well as one of the highest annual day-time and night-time LST and the lowest diurnal difference, was found in the most populous compact low-rise zone. Other zones with a high proportion of both the elderly and children included large low-rise, open-low rise and low plants, with the first two experiencing high temperatures during the day and night. The low plants zone, constituting the rural background of the study area, in contrast, had the lowest night-time LST out of all zones present in the study area, and a medium LST during the day, suggesting relatively low exposure of age-sensitive populations to heat in this zone.

The average income expressed in GDP per capita within the study area was 8159 2017 US $. All built-up zones were characterized by lower-than-average GDP per capita, with only sparsely built marginally exceeding this value, indicating higher heat exposure to economically vulnerable populations. amongst these zones, the compact mid-rise, open mid-rise, and compact low-rise areas had the lowest cooling rates or diurnal LST differences, and high day and night LST, with the lowest per capita incomes at $3203.48, $3786.55, and $4391.06, respectively (Table S9 and S10 in supplementary materials). The highest GDP per capita of 32,441 2017 US $ was observed in the bare rock or paved zone, with the highest day-time and relatively high night-time LST suggesting that some high-earning populations may also be exposed to excess heat, which can, however, be mitigated through better housing and air-conditioning. Other high-income zones included bushes, scattered trees, and bare soil and sand, which comprised the least population in the study area with relatively low exposure to heat during the day and night. Notably, the low plant zones with the third largest population and relatively high income experienced the lowest LST at night, the highest diurnal difference, and a high proportion of children and elderly, indicating that heat-sensitive populations in rural areas are under a lower risk of heat-related discomfort and health issues. It is important to note that high population and GDP per capita were observed in the water zone, which may be due to the coarser spatial resolution of the socio-economic data (1 km) as compared to LCZ (100 m) resulting in mixed pixels, and the concentration of urban economic activity around water bodies.

4. Discussion

4.1. Quantification of landcover in each LCZ

Quantifying the proportion of predominant land cover in each zone is crucial for mitigating heat-related risks and devising planning strategies (Yuan et al., 2022), as the lower spatial resolution of LCZs results in various land cover classes being mixed within each zone despite the LCZ classification being based on urban morphology and land cover (Oliveira, Lopes & Niza, 2020). The results highlight that each local climate zone exhibited a different proportion of land cover, which had implications on the thermal properties of each zone, with significant presence of vegetation in built-up-based local climate zones contributing to alleviation of heat stress and mitigation of excess heat (Fadhil, Hamoodi & Ziboon, 2023; Teo et al., 2022).

The study area predominantly comprised agricultural land, with approximately 70% of the region occupied by low-plant zones. Moreover, more than 25% of the area fell under the built-up class, mainly situated in rural/urban-rural transition regions. This underscores the significance of quantifying land cover classes in each zone for effective heat mitigation planning, as high-heat events also impact rural areas (Sahani, Kumar, Debele & Emmanuel, 2022). Open low-rise spread over 10% of the study region, with 50% of the land cover being vegetation. In contrast to compact built-up areas, open built-up zones and vegetation zones exhibited a higher percentage of vegetation cover, which enhances heat resistance (Hidalgo-García & Rezapouraghdam, 2023). Consequently, these areas are expected to experience low LST during nighttime (Darlington Mushore et al., 2019; Thomas, Sherin, Ansar & Zachariah, 2014), in hot months.

4.2. Annual and seasonal changes in LST over different land cover types

This study examined the variations in diurnal, seasonal and annual LST amongst various land cover types, i.e. built-up, vegetation, and water. The variation in LST is attributed to differences in reflectance and thermal properties of the land cover types (Imran et al., 2021; Xian et al., 2022). Our results demonstrated that vegetation and impervious surfaces influence the magnitude of LST, which varies with weather patterns and time (Chakraborty & Lee, 2019; Mathew, Khandelwal & Kaul, 2018). Outskirt areas with low vegetation or empty land during the day

can exhibit a higher LST than urban areas (Mathew et al., 2018; Mohammad, Goswami & Bonafoni, 2019), and vegetation exhibits fast cooling due to high evapotranspiration during the day and has low heat intensity at night (Meili et al., 2021). These factors led to a more moderate and reduced LST effect during night-time in rural areas than in urban regions. Our findings confirmed that water exhibits high LST at night explained by its ability to accumulate heat until night due to its high heat storage capacity (Steeneveld, Koopmans, Heusinkveld & Theeuwes, 2014).

In comparison to other seasons, higher temperatures were typically observed during the summer and monsoon. Regardless of land cover type, the daily average LST peaked during the summer. Conversely, nighttime average LST peaked during the monsoon season, followed by summer. During summer daytime, direct surface heating (Gao et al., 2019; Ross, Krishnamurti, Pattnaik & Pai, 2018) from solar radiation absorption combined with heat retention from anthropogenic activities (Yang, Ren & Hou, 2019) and heat waves result in elevated LST. Conversely, during the monsoon season, extensive cloud cover acts as a blanket, hindering heat radiation at night. Additionally, high humidity reduces nighttime cooling, thereby increasing monsoon nighttime LST. The urban warming trends were particularly pronounced during summer and monsoon season nights, while cooling trends were observed during winter and post-monsoon seasons. However, during the daytime, warming trends were evident in summer, monsoon, and post-monsoon seasons, which contrasts with prior research indicating urban warming during summer and monsoon seasons and cooling during winter and post-monsoon seasons (Siddiqui et al., 2021). Our study agrees with earlier research highlighting urban heating as being highest during summer and monsoon seasons due to temperature maxima (Imhoff et al., 2010; Siddiqui et al., 2021). It needs to be noted that the monsoon data quality is poor during the day and at night (Supplementary material), which could lead to an inaccurate representation of the LST pattern. Regardless of the data available, much attention should be given to the monsoon month because, according to the Centre for Science and Environment (CSE) research, the monsoon is more thermally uncomfortable than the drier pre-monsoon season/summer season, with summer temperatures 0.3 °C higher than average (Monthly Global Climate Report for Annual 2022, 2023).

The observed decreasing annual trend in day and night LST in 2020 and 2021, followed by an increase in 2022, could be attributed to the various stages of COVID-19 pandemic lockdowns and the subsequent easing of restrictions. Although COVID restrictions were liberalized globally in 2021, the Delhi Disaster Management Authority, Government of NCT of Delhi, issued orders for restricted activities until February 4, 2022, due to several waves (DDMA ORDER, 2022). During the lockdown periods, heat emitted from anthropogenic activities such as transportation, industrial, and human activity decreased, leading to a more significant drop in temperature during the day, aligning with previous studies (Veettil & Van, 2023; Veettil, Puri, Van & Quang, 2023). However, previous studies have not thoroughly examined the nighttime LST patterns during the COVID lockdown period. Nighttime LST is sensitive to urbanization, primarily influenced by heat from solar radiation and anthropogenic activities trapped in the urban canopy during the day, which is then emitted back into the atmosphere at night. This process leads to higher LST in urban areas than in other classes, a phenomenon known as the urban heat island effect (Siddiqui et al., 2021). With the easing of restrictions in 2022, increased daytime anthropogenic activities subsequently influenced nighttime LST (Athukorala & Murayama, 2021; El Kenawy et al., 2020).

4.3. Annual and seasonal changes in LST over different local climate zones

The average LST in compact zones (including compact mid-rise and low-rise areas) was higher as compared to open built-up zones (comprising open mid-rise and low-rise areas) as well as other built-up zones, both diurnally and seasonally due to high heat absorption by the concentrated buildings (Darlington Mushore et al., 2019). However, during the daytime, the compact mid and low-rise zones exhibited the highest average LST, while the compact and open mid-rise zones recorded the highest average LST during nighttime (Thomas et al., 2014), which contradicts the previous research concluding that height has little effect on LST over LCZ (Yang et al., 2020). Tall structures decrease the sky view factor, reducing the amount of radiation lost to outer space (Blake et al., 2011), thereby trapping more heat within the built-up area and intensifying surface warming during the night. The study aligns with previous research that open, low-rise and sparsely built LCZs are cooler than compact and mid-rise LCZs at night (Kotharkar & Bagade, 2018a). Interestingly, during the post-monsoon period, the average LST during the day for both open and compact low-rise buildings surpassed that of the mid-rise zone. We found a significant difference in LST for large low-rise areas, particularly with the highest LST, especially during nighttime, which contradicts previous research where the large low-rise had the highest mean LST in all seasons amongst all built-up types (Du et al., 2020).

Local climate zones with the highest diurnal temperature difference exhibited the fastest cooling capacity. LCZs without tall features showed a high diurnal difference (Danniswari, Honjo & Furuya, 2022), followed by low-height and medium-height zones. This is because tall features such as buildings and trees trap heat in their canopies during the day and emit it back at night, a process that is much less pronounced in flat, open areas. Densely built-up areas, such as compact mid-rise and compact low-rise, retained heat more effectively than less dense ones within the same height category. These results add to the finding that taller buildings contribute to lower LST in the mornings (Danniswari et al., 2022), which the specificity of the thermal response of buildings with varied morphologies at different times of the day could explain.

4.4. Socio-economic vulnerability to LST within LCZs

Our results indicate that a larger proportion of the population resides in built-up areas, which are more vulnerable to heat-related challenges (Cai, Tang & Zhan, 2021; de Schrijver et al., 2023). The built-up-based LCZs exhibit a dense population distribution (Cai et al., 2021), with a consistent pattern observed across all three age and vulnerability classes: children, adults, and the elderly. Children and the elderly are more susceptible to increased LST than adults in good health (Piracha & Chaudhary, 2022). Compared to scattered built-up, other built-up zones accommodate the highest percentage of the population (Zhu et al., 2022). The sensitivity to heat varies amongst individuals, with higher risks primarily observed amongst disadvantaged populations due to age differences, underlying medical conditions, economic conditions, and other factors (Chang, Tan, Nadeau & Odden, 2022; Huang et al., 2023; van Daalen et al., 2022).

Furthermore, in our study region, 30% of the population lived in the compact zones affected by more intensive heat, where the GDP is less than 20%. The compact zones are likely to predominantly consist of slums, marked by the low quality of life, economic hardship, and insufficient housing conditions (Banerji, Bhattacharjea & Wadhwa, 2013; J. Chen et al., 2016; Directorate of economics & statistics, 2015), exposing their inhabitants to excessive heat levels compared to their immediate surroundings (Wang, Kuffer, Sliuzas & Kohli, 2019). These findings are consistent with apparent social inequities in access to greenspaces (Pham, Apparicio, Séguin, Landry & Gagnon, 2012) and greater heat exposure related to class disparities (Benz & Burney, 2021) observed in North America. Conversely, more affluent populations inhabiting rural areas experienced lower heat exposure than less affluent city dwellers. It needs to be noted, however, that both high and low-income populations may be less exposed to excess heat, depending on socio-ecological settings (Shih, 2022).

5. Limitations

The primary set of limitations of our study concerns varied spatial resolutions of spatial data in a raster format used for the analysis. LST was available at 1 km, LCZs at 100 m and LC at 30 m, which resulted in scale mismatches and the need to aggregate the finer resolution data, causing the presence of mixed pixels affecting the thermal response of contrasting LCs and LCZs. Aggregation of the LC and LCZ data to match the LST at a coarser resolution could have also resulted in a loss of thermal effects occurring at finer scales. Future research efforts should, therefore, aim to improve the spatial resolution of LST data, such as by the use of LST downscaling algorithms (Bala, Prasad & Yadav, 2020), ensuring compatibility with the fine-scale landcover and LCZ classification. This could help determine thermal extremes and corresponding urban morphology patterns with enhanced detail as compared to the values averaged over 1 × 1 km of land parcels. Similar considerations apply to the GDP and population data, where coarse spatial resolution and scale mismatches could have resulted in erroneous attributions of socio-economic factors to the different urban morphologies. Despite these limitations, our study represents major trends in the relationships between different urban landscapes and thermal and socio-economic properties.

Another important factor to consider is the completeness of LST data. Whilst MODIS provides daily and diurnal LST data, it is noteworthy that during the winter and monsoon seasons, a considerable number of pixels were obscured by cloud cover and, therefore, removed, potentially affecting the accuracy of the analysis (Figure S11 in supplementary materials).

Furthermore, the analysis related to socio-economic factors to heat exposure does not account for adult populations with medical histories vulnerable to heat. Also, diurnal shifts in population due to commuting during the day and night are not considered. Moreover, more spatially precise demographic and household income data could provide further insights into the heat exposure of different social groups within the different built-up-based LCZs to investigate heat-related social inequities in further detail within the urbanized portion of the study region.

6. Conclusion

Our study examined the impact of diurnal changes in land surface temperature on an annual and seasonal basis within different land cover types and local climate zones present in the greater Delhi region in India on age-sensitive and economically vulnerable populations. We found that local climate zones with taller features, both built-up and natural, experienced higher temperatures during the day and night than their lower counterparts and had lower diurnal differences in LST, which indicates lower heat respite during the night. Additionally, an increase in urban density further reduced the diurnal difference. amongst these zones, taller and more densely built-up urban features exhibited higher diurnal differences in LST compared to tall, densely vegetated zones in all seasons except the monsoon. Considering seasonality, the highest day-time LST was observed in the summer, whilst night-time LST in the monsoon. The night-time cooling was generally higher in vegetated local climate zones except for the monsoon, when it was higher in urban areas. Our study also found that a high proportion of children and the elderly inhabited urban zones most prone to urban heating, which were more economically vulnerable than rural zones characterized by lower heat exposure. This study enriches the existing body of literature with further evidence for social inequity in terms of access to urban cooling, as well as provides insights into the urban form morphologies that are conducive to more thermally comfortable environment. Short-term mitigation planning during extreme heat events could be focused on high-rise and densely urban-based LCZs rather than the entire city area, as these zones have high population counts and are more vulnerable to heat stress. To promote health and well-being, future urban development should consider adopting sparsely built, open or large low-rise structures with low plants to prevent overheating.

CRediT authorship contribution statement

Prathiba A. Palanisamy: Writing – original draft, Visualization, Methodology, Formal analysis, Conceptualization. **Joanna Zawadzka:** Writing – review & editing, Validation, Supervision, Methodology, Conceptualization. **Kamal Jain:** Writing – review & editing, Supervision. **Stefania Bonafoni:** Writing – review & editing, Supervision. **Anuj Tiwari:** Writing – review & editing, Formal analysis.

Declaration of competing interest

The authors declare no conflicts of interest.

Acknowledgment

The authors express their sincere gratitude to the Commonwealth Split-Site Scholarship for providing a fellowship to Prathiba A. Palanisamy. This support facilitated the research conducted at Cranfield University, UK, during the tenure of the scholarship.

Supplementary materials

Supplementary material associated with this article can be found, in the online version, at doi:10.1016/j.scs.2024.105880.

Data availability

All the data utilized in the study are openly accessible, and the manuscript includes citations to the respective links or articles from which the data were sourced

References

Abbasi, B., Qin, Z., Du, W., Li, S., Fan, J., & Zhao, S. (2020). Effects of cloud on land surface temperature (LST) change in thermal infrared remote sensing images: A case study of landsat 8 data. In *International Geoscience and Remote Sensing Symposium (IGARSS)* (pp. 5430–5433). https://doi.org/10.1109/IGARSS39084.2020.9324415

Abdullah, S., Barua, D., Abdullah, S. M. A., & Rabby, Y. W. (2022). Investigating the impact of land Use/Land cover change on present and future land surface temperature (LST) of Chittagong, Bangladesh. *Earth Systems and Environment, 6*(1), 221–235. https://doi.org/10.1007/S41748-021-00291-W/FIGURES/10

Athukorala, D., & Murayama, Y. (2021). Urban heat island formation in greater cairo: spatio-temporal analysis of daytime and nighttime land surface temperatures along the urban–rural gradient. *Remote Sensing, 13*(7), 1396. https://doi.org/10.3390/RS13071396

Bala, R., Prasad, R., & Yadav, V. P. (2020). Thermal sharpening of MODIS land surface temperature using statistical downscaling technique in urban areas. *Theoretical and Applied Climatology, 141*(3–4), 935–946. https://doi.org/10.1007/S00704-020-03253-W/FIGURES/8

Banerji, R., Bhattacharjea, S., & Wadhwa, W. (2013). The annual status of education report (ASER). *Research in Comparative and International Education, 8*(3), 387–396. https://doi.org/10.2304/RCIE.2013.8.3.387

Benz, S. A., & Burney, J. A. (2021). Widespread race and class disparities in surface urban heat extremes across the United States. *Earth's Future, 9*(7), Article e2021EF002016. https://doi.org/10.1029/2021EF002016

Blake, R., Grimm, A., Ichinose, T., Horton, R., Gaffi, S., Jiong, S., Bader, D., Cecil, L. D., & Blake, R. (2011). Urban climate: Processes, trends, and projections. *Climate Change and Cities: First Assessment Report of the Urban Climate Change Research Network*, 43–81.

Bondarenko, M., Kerr, D., Sorichetta, A., & Tatem, A. (2020).& WorldPop.*Estimates of 2020 total number of people per grid square, adjusted to match the corresponding UNPD 2020 estimates and broken down by gender and age groupings, produced using Built-Settlement Growth Model (BSGM) outputs*. https://doi.org/10.5258/SOTON/WP00698.

Breil, M., Davin, E. L., & Rechid, D. (2021). What determines the sign of the evapotranspiration response to afforestation in European summer? *Biogeosciences (Online), 18*(4), 1499–1510. https://doi.org/10.5194/BG-18-1499-2021

Business Standard. (2024,. June 20). *Amid heatwave, Delhi govt orders rescue of homeless from footpaths, parks | India News - Business Standard*. https://www.business-standard.com/india-news/amid-heatwave-delhi-govt-orders-rescue-of-homeless-from-footpaths-parks-124062000897_1.html.

Cai, Z., Tang, Y., & Zhan, Q. (2021). A cooled city? Comparing human activity changes on the impact of urban thermal environment before and after city-wide lockdown.

Building and Environment, 195, Article 107729. https://doi.org/10.1016/J.BUILDENV.2021.107729
Chakraborty, T., & Lee, X. (2019). A simplified urban-extent algorithm to characterize surface urban heat islands on a global scale and examine vegetation control on their spatiotemporal variability. *International Journal of Applied Earth Observation and Geoinformation, 74*, 269–280. https://doi.org/10.1016/J.JAG.2018.09.015
Chang, A. Y., Tan, A. X., Nadeau, K. C., & Odden, M. C. (2022). Aging hearts in a hotter, more turbulent world: The impacts of climate change on the cardiovascular health of older adults. *Current Cardiology Reports, 24*(6), 749–760. https://doi.org/10.1007/S11886-022-01693-6
Chatterjee, U., & Majumdar, S. (2022). Impact of land use change and rapid urbanization on urban heat island in Kolkata city: A remote sensing based perspective. *Journal of Urban Management, 11*(1), 59–71. https://doi.org/10.1016/J.JUM.2021.09.002
Chauhan, S., & Jethoo, A. S. (2023). Statistical analysis of diurnal variations in land surface temperature and the UHI effect using aqua and terra MODIS data. *Remote Sensing Letters, 14*(5), 503–511. https://doi.org/10.1080/2150704X.2023.2215948
Chen, J., Chu, S., Chungbaek, Y., Khan, M., Kuhlman, C., Marathe, A., Mortveit, H., Vullikanti, A., & Xie, D. (2016). Effect of modelling slum populations on influenza spread in Delhi. *BMJ open, 6*(9), Article e011699. https://doi.org/10.1136/BMJOPEN-2016-011699
Chen, J., Gao, M., Cheng, S., Hou, W., Song, M., Liu, X., et al. (2022). Global 1 km × 1 km gridded revised real gross domestic product and electricity consumption during 1992–2019 based on calibrated nighttime light data. *Scientific Data, 9*, Article 202. https://doi.org/10.1038/s41597-022-01322-5
Chen, Y., Yang, J., Yu, W., Ren, J., Xiao, X., & Xia, J. C. (2023). Relationship between urban spatial form and seasonal land surface temperature under different grid scales. *Sustainable Cities and Society, 89*, Article 104374. https://doi.org/10.1016/j.scs.2022.104374
Climate data. (2022). *New delhi climate: Temperature new delhi & weather by month*. CLIMATE DATA FOR CITIES WORLDWIDE. https://en.climate-data.org/asia/india/delhi/new-delhi-30/#temperature-graph.
Cloud Cover Data of Delhi. (2018). Indian Climate. https://www.indianclimate.com/cloud-cover-data.php?request=5DWH4PLGSL.
Danniswari, D., Honjo, T., & Furuya, K. (2022). Analysis of building height impact on land surface temperature by digital building height model obtained from AW3D30 and SRTM. *Geographies, 2*(4), 563–576. https://doi.org/10.3390/GEOGRAPHIES2040034. *2022, Vol. 2, Pages 563-576*.
Darlington Mushore, T., Dube, T., Manjowe, M., Gumindoga, W., Chemura, A., Rousta, I., Odindi, J., & Mutanga, O. (2019). Remotely sensed retrieval of Local Climate Zones and their linkages to land surface temperature in Harare metropolitan city, Zimbabwe. *Urban Climate, 27*, 259–271. https://doi.org/10.1016/j.uclim.2018.12.006
Das, M., & Das, A. (2020). Assessing the relationship between local climatic zones (LCZs) and land surface temperature (LST) – A case study of Sriniketan-Santiniketan Planning Area (SSPA), West Bengal, India. *Urban Climate, 32*, Article 100591. https://doi.org/10.1016/J.UCLIM.2020.100591
DDMA ORDER. (2022). Delhi Disaster Management Authority. https://ddma.delhi.gov.in/doit-tabcontent/ddma-order.
Demuzere, M., Kittner, J., Martilli, A., Mills, G., Moede, C., Stewart, I. D., Van Vliet, J., & Bechtel, B. (2022). A global map of local climate zones to support earth system modelling and urban-scale environmental science. *Earth System Science Data, 14*(8), 3835–3873. https://doi.org/10.5194/ESSD-14-3835-2022
Denager, T., Looms, M. C., Sonnenborg, T. O., & Jensen, K. H. (2020). Comparison of evapotranspiration estimates using the water balance and the eddy covariance methods. *Vadose Zone Journal, 19*(1), Article e20032. https://doi.org/10.1002/VZJ2.20032
Dewan, A., Kiselev, G., & Botje, D. (2021). Diurnal and seasonal trends and associated determinants of surface urban heat islands in large Bangladesh cities. *Applied Geography, 135*, Article 102533. https://doi.org/10.1016/j.apgeog.2021.102533
Directorate of economics & statistics. (2015). *Urban Slums in Delhi*. http://des.delhigovt.nic.in.
Du, P., Chen, J., Bai, X., & Han, W. (2020). Understanding the seasonal variations of land surface temperature in Nanjing urban area based on local climate zone. *Urban Climate, 33*, Article 100657. https://doi.org/10.1016/J.UCLIM.2020.100657
El Kenawy, A. M., Hereher, M., Robaa, S. M., McCabe, M. F., Lopez-Moreno, J. I., Domínguez-Castro, F., Gaber, I. M., Al-Awadhi, T., Al-Buloshi, A., Nasiri, N. Al, Al-Hatrushi, S., Schuwerack, P. M., Peña-Angulo, D., Abdelaal, M. M., & Vicente-Serrano, S. M. (2020). Nocturnal surface urban heat island over greater cairo: Spatial morphology, temporal trends and links to land-atmosphere influences. *Remote Sensing, 12*(23), 3889. https://doi.org/10.3390/RS12233889. *2020, Vol. 12, Page 3889*.
Fadhil, M., Hamoodi, M. N., & Ziboon, A. R. T. (2023). Mitigating urban heat island effects in urban environments: Strategies and tools. In *, 1129. IOP Conference Series: Earth and Environmental Science*, Article 012025. https://doi.org/10.1088/1755-1315/1129/1/012025
Feng, Z., Wang, X., Yuan, J., Zhang, Y., & Yu, M. (2023). Changes in air pollution, land surface temperature, and urban heat islands during the COVID-19 lockdown in three Chinese urban agglomerations. *Science of The Total Environment, 892*, Article 164496. https://doi.org/10.1016/J.SCITOTENV.2023.164496
Gao, Z., Hou, Y., & Chen, W. (2019). Enhanced sensitivity of the urban heat island effect to summer temperatures induced by urban expansion. *Environmental Research Letters, 14*(9), Article 094005. https://doi.org/10.1088/1748-9326/ab2740
Guha, S., & Govil, H. (2021). COVID-19 lockdown effect on land surface temperature and normalized difference vegetation index. *Geomatics, natural hazards and risk, 12*(1), 1082–1100. https://doi.org/10.1080/19475705.2021.1914197
Guo, L., Di, L., Zhang, C., Lin, L., Chen, F., & Molla, A. (2022). Evaluating contributions of urbanization and global climate change to urban land surface temperature change: A case study in Lagos, Nigeria. *Scientific Reports, 12*, 14168. https://doi.org/10.1038/s41598-022-18193-w
Hamed Fahmy, A., Amin Abdelfatah, M., & El-Fiky, G. (2023). Investigating land use land cover changes and their effects on land surface temperature and urban heat islands in Sharqiyah Governorate, Egypt. *The Egyptian Journal of Remote Sensing and Space Sciences, 26*, 293–306. https://doi.org/10.1016/j.ejrs.2023.04.001
Hidalgo-García, D., & Rezapouraghdam, H. (2023). Variability of heat stress using the UrbClim climate model in the city of Seville (Spain): Mitigation proposal. *Environmental Monitoring and Assessment, 195*(10), 1–26. https://doi.org/10.1007/S10661-023-11768-8/TABLES/9
Hsu, A., Sheriff, G., Chakraborty, T., & Manya, D. (2021). Disproportionate exposure to urban heat island intensity across major US cities. *Nature Communications, 12*(1), 1–11. https://doi.org/10.1038/s41467-021-22799-5. *2021 12:1*.
Hu, J., Zhao, T., Liu, J., Cao, L., Xia, J., Wang, C., Zhao, X., Gao, Z., Shu, Z., & Li, Y. (2021). Nocturnal surface radiation cooling modulated by cloud cover change reinforces PM2.5 accumulation: Observational study of heavy air pollution in the Sichuan Basin, Southwest China. *Science of The Total Environment, 794*, Article 148624. https://doi.org/10.1016/J.SCITOTENV.2021.148624
Huang, W. T. K., Masselot, P., Bou-Zeid, E., Fatichi, S., Paschalis, A., Sun, T., Gasparrini, A., & Manoli, G. (2023). Economic valuation of temperature-related mortality attributed to urban heat islands in European cities. *Nature Communications, 14*(1), 1–12. https://doi.org/10.1038/s41467-023-43135-z
Imhoff, M. L., Zhang, P., Wolfe, R. E., & Bounoua, L. (2010). Remote sensing of the urban heat island effect across biomes in the continental USA. *Remote Sensing of Environment, 114*(3), 504–513.
Imran, H. M., Hossain, A., Islam, A. K. M. S., Rahman, A., Bhuiyan, M. A. E., Paul, S., & Alam, A. (2021). Impact of Land Cover Changes on Land Surface Temperature and Human Thermal Comfort in Dhaka City of Bangladesh. *Earth Systems and Environment, 5*(3), 667–693. https://doi.org/10.1007/S41748-021-00243-4/FIGURES/10
Intergovernmental Panel on Climate Change. (2021). *Climate Change 2021*. www.ipcc.ch.
Javaid, K., Ghafoor, G. Z., Sharif, F., Shahid, M. G., Shahzad, L., Ghafoor, N., Hayyat, M. U., & Farhan, M. (2023). Spatio-temporal analysis of land use land cover change and its impact on land surface temperature of Sialkot City, Pakistan. *Scientific Reports, 13*(1), 1–15. https://doi.org/10.1038/s41598-023-49608-x. *2023 13:1*.
Kafy, A. Al, Rahman, M. S., Faisal, A. Al, Hasan, M. M., & Islam, M. (2020). Modelling future land use land cover changes and their impacts on land surface temperatures in Rajshahi, Bangladesh. *Remote Sensing Applications: Society and Environment, 18*, Article 100314. https://doi.org/10.1016/J.RSASE.2020.100314
Kafy, A. Al, Saha, M., Faisal, A. Al, Rahaman, Z. A., Rahman, M. T., Liu, D., … Ahasan, M. A. K. (2022). Predicting the impacts of land use/land cover changes on seasonal urban thermal characteristics using machine learning algorithms. *Building and Environment, 217*, Article 109066. https://doi.org/10.1016/J.BUILDENV.2022.109066
Kimothi, S., Thapliyal, A., Gehlot, A., Aledaily, A. N., gupta, A., Bilandi, N., Singh, R., Kumar Malik, P., & Vaseem Akram, S. (2023). Spatio-temporal fluctuations analysis of land surface temperature (LST) using Remote Sensing data (LANDSAT TM5/8) and multifractal technique to characterize the urban heat Islands (UHIs). *Sustainable Energy Technologies and Assessments, 55*, Article 102956. https://doi.org/10.1016/J.SETA.2022.102956
Kotharkar, R., & Bagade, A. (2018). Evaluating urban heat island in the critical local climate zones of an Indian city. *Landscape and Urban Planning, 169*, 92–104. https://doi.org/10.1016/J.LANDURBPLAN.2017.08.009
Kotharkar, R., Ghosh, A., & Kotharkar, V. (2021). Estimating summertime heat stress in a tropical Indian city using Local Climate Zone (LCZ) framework. *Urban Climate, 36*, Article 100784. https://doi.org/10.1016/J.UCLIM.2021.100784
Kumar, A., Agarwal, V., Pal, L., Chandniha, S. K., & Mishra, V. (2021). Effect of land surface temperature on urban heat Island in Varanasi City, India. *J, 4*(3), 420–429. https://doi.org/10.3390/J4030032. *2021, Vol. 4, Pages 420-429*.
Li, K., Lyu, D., Chen, Y., & Jiang, J. (2024). Classifying seasonal patterns of clear-sky surface urban heat island worldwide and investigating impacts from surface energy variations. *Sustainable Cities and Society, 106*, Article 105367. https://doi.org/10.1016/J.SCS.2024.105367
Li, Y., Sun, Y., Li, J., & Gao, C. (2020). Socioeconomic drivers of urban heat island effect: Empirical evidence from major Chinese cities. *Sustainable Cities and Society, 63*, Article 102425. https://doi.org/10.1016/j.scs.2020.102425
Maharjan, M., Aryal, A., Man Shakya, B., Talchabhadel, R., Thapa, B. R., & Kumar, S. (2021). Evaluation of Urban Heat Island (UHI) Using Satellite Images in Densely Populated Cities of South Asia. *Earth, 2*(1), 86–110. https://doi.org/10.3390/EARTH2010006. *2021, Vol. 2, Pages 86-110*.
Mathew, A., Khandelwal, S., & Kaul, N. (2018). Analysis of diurnal surface temperature variations for the assessment of surface urban heat island effect over Indian cities. *Energy & Buildings, 159*, 271–295. https://doi.org/10.1016/j.enbuild.2017.10.062
Meili, N., Manoli, G., Burlando, P., Carmeliet, J., Chow, W. T. L., Coutts, A. M., Roth, M., Velasco, E., Vivoni, E. R., & Fatichi, S. (2021). Tree effects on urban microclimate: Diurnal, seasonal, and climatic temperature differences explained by separating radiation, evapotranspiration, and roughness effects. *Urban Forestry & Urban Greening, 58*, 1618–8667. https://doi.org/10.1016/j.ufug.2020.126970
Mohammad, P., Goswami, A., & Bonafoni, S. (2019). *The Impact of the Land Cover Dynamics on Surface Urban Heat Island Variations in Semi-Arid Cities: A Case Study in Ahmedabad City, India, Using Multi-Sensor/Source Data*. https://doi.org/10.3390/s19173701.

Mohan, M., Sati, A. P., & Bhati, S. (2020). Urban sprawl during five decadal period over National Capital Region of India: Impact on urban heat island and thermal comfort. *Urban Climate, 33*, Article 100647. https://doi.org/10.1016/j.uclim.2020.100647

Monthly Global Climate Report for Annual 2022. (2023,. January). NOAA National Centers for Environmental Information.

Morabito, M., Crisci, A., Guerri, G., Messeri, A., Congedo, L., & Munafò, M. (2021). Surface urban heat islands in Italian metropolitan cities: Tree cover and impervious surface influences. *Science of The Total Environment, 751*, Article 142334. https://doi.org/10.1016/J.SCITOTENV.2020.142334

NITI Aayog, & Asian Development Bank. (2022). *Cities as Engines of Growth*. https://doi.org/10.1093/wber/lhab022.

Oliveira, A., Lopes, A., & Niza, S. (2020). Local climate zones classification method from Copernicus land monitoring service datasets: An ArcGIS-based toolbox. *MethodsX, 7*, Article 101150. https://doi.org/10.1016/j.uclim.2020.100631

Palanisamy, P. A., Zawadzka, J., Jain, K., & Bonafoni, S. (2023). Monitoring summer daytime and nighttime decadal trends of land surface temperature over the national capital region DELHI. *The International Archives of the Photogrammetry, Remote Sensing and Spatial Information Sciences, XLVIII-1-W2-2023(1/W2-2023)*, 1491–1497. https://doi.org/10.5194/ISPRS-ARCHIVES-XLVIII-1-W2-2023-1491-2023

Palanisamy, P.A., Jain, K., & Bonafoni, S. (2023). *Machine Learning Classifier Evaluation for Different Input Combinations : A Case Study with Landsat 9 and Sentinel-2 Data*.

Parvar, Z., Mohammadzadeh, M., & Saeidi, S. (2024). LCZ framework and landscape metrics: Exploration of urban and peri-urban thermal environment emphasizing 2/3D characteristics. *Building and Environment, 254*, Article 111370. https://doi.org/10.1016/J.BUILDENV.2024.111370

Pham, T. T. H., Apparicio, P., Séguin, A. M., Landry, S., & Gagnon, M. (2012). Spatial distribution of vegetation in Montreal: An uneven distribution or environmental inequity? *Landscape and Urban Planning, 107*(3), 214–224. https://doi.org/10.1016/J.LANDURBPLAN.2012.06.002

Piracha, A., & Chaudhary, M. T. (2022). Urban air pollution, urban heat island and human health: A review of the literature. *Sustainability, 14*(15), 9234. https://doi.org/10.3390/SU14159234

Ross, R. S., Krishnamurti, T. N., Pattnaik, S., & Pai, D. S. (2018). Decadal surface temperature trends in India based on a new high-resolution data set. *Scientific Reports, 8*(1), 1–10. https://doi.org/10.1038/s41598-018-25347-2. *2018 8:1*.

Rydin, Y., Bleahu, A., Davies, M., Dávila, J. D., Friel, S., De Grandis, G., … Wilson, J. (2012). Shaping cities for health: Complexity and the planning of urban environments in the 21st century. In *The lancet, 379*. London, United Kingdom: Elsevier B.V.. https://doi.org/10.1016/S0140-6736(12)60435-8

Sahani, J., Kumar, P., Debele, S., & Emmanuel, R. (2022). Heat risk of mortality in two different regions of the United Kingdom. *Sustainable Cities and Society, 80*, Article 103758. https://doi.org/10.1016/j.scs.2022.103758

Schrijver, E.de, Royé, D., Gasparrini, A., Franco, O. H., & Vicedo-Cabrera, A. M. (2023). Exploring vulnerability to heat and cold across urban and rural populations in Switzerland. *Environmental Research: Health, 1*(2), Article 025003. https://doi.org/10.1088/2752-5309/acab78

Shahfahad, Naikoo, M. W., Towfiqul Islam, A. R. M., Mallick, J., & Rahman, A. (2022). Land use/land cover change and its impact on surface urban heat island and urban thermal comfort in a metropolitan city. *Urban Climate, 41*, Article 101052. https://doi.org/10.1016/J.UCLIM.2021.101052

Sharma, S., Dass, A., Mishra, A. K., Singh, S., & Kumar, K. (2022). A decadal climatology of cloud vertical structure over the Indo-Gangetic Plain using radiosonde and radar observations. *Atmospheric Research, 266*, Article 105949. https://doi.org/10.1016/J.ATMOSRES.2021.105949

Shih, W. Y. (2022). Socio-ecological inequality in heat: The role of green infrastructure in a subtropical city context. *Landscape and Urban Planning, 226*, Article 104506. https://doi.org/10.1016/J.LANDURBPLAN.2022.104506

Shukla, A., & Jain, K. (2021). Analyzing the impact of changing landscape pattern and dynamics on land surface temperature in Lucknow city, India. *Urban Forestry & Urban Greening, 58*, Article 126877. https://doi.org/10.1016/J.UFUG.2020.126877

Siddiqui, A., Kushwaha, G., Nikam, B., Srivastav, S. K., Shelar, A., & Kumar, P. (2021). Analysing the day/night seasonal and annual changes and trends in land surface temperature and surface urban heat island intensity (SUHII) for Indian cities. *Sustainable Cities and Society, 75*. https://doi.org/10.1016/j.scs.2021.103374, 103374.

Steeneveld, G. J., Koopmans, S., Heusinkveld, B. G., & Theeuwes, N. E. (2014). Refreshing the role of open water surfaces on mitigating the maximum urban heat island effect. *Landscape and Urban Planning, 121*, 92–96. https://doi.org/10.1016/j.landurbplan.2013.09.001

Stewart, I. D., & Oke, T. R. (2012). Local climate zones for urban temperature studies. *Bulletin of the American Meteorological Society, 93*(12), 1879–1900. https://doi.org/10.1175/BAMS-D-11-00019.1

Teo, Y. H., Makani, M. A. B. H., Wang, W., Liu, L., Yap, J. H., & Cheong, K. H. (2022). Urban heat Island mitigation: GIS-based analysis for a tropical city Singapore. *International Journal of Environmental Research and Public Health, 19*(19), Article 11917. https://doi.org/10.3390/IJERPH191911917/S1

Thomas, G., Sherin, A. P., Ansar, S., & Zachariah, E. J. (2014). Analysis of urban heat Island in Kochi, India, Using a modified local climate zone classification. *Procedia Environmental Sciences, 21*, 3–13. https://doi.org/10.1016/J.PROENV.2014.09.002

Ullah, N., Siddique, M. A., Ding, M., Grigoryan, S., Khan, I. A., Kang, Z., … Zhang, Y. (2023). The impact of urbanization on urban heat island: predictive approach using google earth engine and CA-Markov Modelling (2005–2050) of Tianjin City, China. *International Journal of Environmental Research and Public Health, 20*(3), 2642. https://doi.org/10.3390/IJERPH20032642

Unal Cilek, M., & Cilek, A. (2021). Analyses of land surface temperature (LST) variability among local climate zones (LCZs) comparing Landsat-8 and ENVI-met model data. *Sustainable Cities and Society, 69*, Article 102877. https://doi.org/10.1016/J.SCS.2021.102877

van Daalen, K. R., Romanello, M., Rocklöv, J., Semenza, J. C., Tonne, C., Markandya, A., Dasandi, N., Jankin, S., Achebak, H., Ballester, J., Bechara, H., Callaghan, M. W., Chambers, J., Dasgupta, S., Drummond, P., Farooq, Z., Gasparyan, O., Gonzalez-Reviriego, N., Hamilton, I., … Lowe, R. (2022). The 2022 europe report of the lancet countdown on health and climate change: Towards a climate resilient future. *The Lancet Public Health, 7*(11), e942–e965. https://doi.org/10.1016/S2468-2667(22)00197-9

Veettil, B. K., Puri, V., Van, D. D., & Quang, N. X. (2023). Variations in land surface temperatures in small-scale urban areas in Vietnam during Covid-19 restrictions: Case studies from Da Nang, Hue and Vinh City. *Environmental Monitoring and Assessment, 195*(7), 1–19. https://doi.org/10.1007/S10661-023-11332-4/FIGURES/6

Veettil, B. K., & Van, D. D. (2023). Did the Covid-19 restrictions influence land surface temperatures in Southeast Asia? A study from Ho Chi Minh City, Vietnam. *Environmental Science and Pollution Research, 30*(25), 66812–66821. https://doi.org/10.1007/S11356-023-26892-8/FIGURES/6

Wang, J., Kuffer, M., Sliuzas, R., & Kohli, D. (2019). The exposure of slums to high temperature: Morphology-based local scale thermal patterns. *Science of The Total Environment, 650*, 1805–1817. https://doi.org/10.1016/J.SCITOTENV.2018.09.324

Wang, Z., Ishida, Y., & Mochida, A. (2023). Effective Factors for Reducing Land Surface Temperature in Each Local Climate Zone Built Type in Tokyo and Shanghai. *Remote Sensing, 15*(15), 3840. https://doi.org/10.3390/RS15153840

World Health Organization. (2014). *Quantitative risk assessment of the effects of climate change on selected causes of death, 2030s and 2050s*. https://apps.who.int/iris/bitstream/handle/10665/134014/9789241507691_eng.pdf.

WorldPop. (2020). *Global development data - WorldPop*. https://www.worldpop.org/datacatalog/.

Xian, G., Shi, H., Zhou, Q., Auch, R., Gallo, K., Wu, Z., et al. (2022). Monitoring and characterizing multi-decadal variations of urban thermal condition using time-series thermal remote sensing and dynamic land cover data. *Remote Sensing of Environment, 269*, Article 112803. https://doi.org/10.1016/j.rse.2021.112803

Xin, J., Yang, J., Sun, D., Han, T., Song, C., & Shi, Z. (2022). Seasonal differences in land surface temperature under different land Use/Land cover types from the perspective of different climate Zones. *Land, 11*(8), 1122. https://doi.org/10.3390/LAND11081122

Yang, J., Zhan, Y., Xiao, X., Xia, J. C., Sun, W., & Li, X. (2020). Investigating the diversity of land surface temperature characteristics in different scale cities based on local climate zones. *Urban Climate, 34*, Article 100700. https://doi.org/10.1016/J.UCLIM.2020.100700

Yang, P., Ren, G., & Hou, W. (2019). Impact of daytime precipitation duration on urban heat island intensity over Beijing city. *Urban Climate, 28*, Article 100463. https://doi.org/10.1016/j.uclim.2019.100463

Yuan, B., Li, X., Zhou, L., Bai, T., Hu, T., Huang, J., et al. (2023). Global distinct variations of surface urban heat islands in inter- and intra-cities revealed by local climate zones and seamless daily land surface temperature data. *ISPRS Journal of Photogrammetry and Remote Sensing, 204*, 1–14. https://doi.org/10.1016/J.ISPRSJPRS.2023.08.012

Yuan, B., Zhou, L., Hu, F., & Zhang, Q. (2022). Diurnal dynamics of heat exposure in Xi'an: A perspective from local climate zone. *Building and Environment, 222*, Article 109400. https://doi.org/10.1016/J.BUILDENV.2022.109400

Zhao, W., & Duan, S. B. (2020). Reconstruction of daytime land surface temperatures under cloud-covered conditions using integrated MODIS/Terra land products and MSG geostationary satellite data. *Remote Sensing of Environment, 247*, Article 111931. https://doi.org/10.1016/J.RSE.2020.111931

Zheng, Y., Ren, C., Shi, Y., Yim, S. H. L., Lai, D. Y. F., Xu, Y., Fang, C., & Li, W. (2023). Mapping the spatial distribution of nocturnal urban heat island based on Local Climate Zone framework. *Building and Environment, 234*, Article 110197. https://doi.org/10.1016/j.buildenv.2023.110197

Zhu, X. X., Qiu, C., Hu, J., Shi, Y., Wang, Y., Schmitt, M., & Taubenböck, H. (2022). The urban morphology on our planet – Global perspectives from space. *Remote Sensing of Environment, 269*, Article 112794. https://doi.org/10.1016/J.RSE.2021.112794

Zwolska, A., Półrolniczak, M., & Kolendowicz, L. (2024). Urban growth's implications on land surface temperature in a medium-sized European city based on LCZ classification. *Scientific Reports, 14*(1), 1–14. https://doi.org/10.1038/s41598-024-58501-0. *2024 14:1*.



https://dspace.org/

Assessing diurnal land surface temperature variations across landcover and local climate zones: implications for urban planning and mitigation strategies on socio-economic factors

Palanisamy, Prathiba A.; Zawadzka, Joanna Ewa; Jain, Kamal; Bonafoni, Stefania; Tiwari, Anuj

2024-12-01
Elsevier
https://doi.org/10.1016/j.scs.2024.105880
Palanisamy PA, Zawadzka J, Jain K, et al., (2024) Assessing diurnal land surface temperature variations across landcover and local climate zones: implications for urban planning and mitigation strategies on socio-economic factors. Sustainable Cities and Society, Volume 116, December 2024, Article number 105880

Downloaded from a DSpace repository. https://dspace.org/